공학석사 학위논문

Failure of Transversely Isotropic Rocks Under Intermediate Strain Rate Loading

중간변형률속도 재하에서의
횡등방성 암석의 파괴 거동

2022년 2월

서울대학교 대학원
에너지시스템공학부
이 원 희

Failure of Transversely Isotropic Rocks Under Intermediate Strain Rate Loading

중간변형률속도 재하에서의
횡등방성 암석의 파괴 거동

지도 교수 전 석 원

이 논문을 공학석사 학위논문으로 제출함
2022 년 2 월

서울대학교 대학원
에너지시스템공학부
이 원 희

이원희의 공학석사 학위논문을 인준함
2022 년 2 월

위 원 장 송 재 준 (인)

부위원장 전 석 원 (인)

위 원 민 기 복 (인)

Abstract

Wonhi Lee
Department of Energy Systems Engineering
The Graduate School
Seoul National University

Rocks involved with mechanized excavation via moving rock cutting tools are known to be under the influence of intermediate strain rate loading. In the mechanical excavation of rock, the cutting efficiency is affected by discontinuities, while the density of discontinuities and the direction of excavation against discontinuities greatly affect the efficiency of cutting. However, the deformation and fracture behavior of rocks vary depending on the changes in loading rate. It is known that under higher loading rates, rocks show relatively higher strength and low anisotropic behaviors. In this research, strength properties under static and intermediate strain rate loadings were studied using transversely isotropic rocks and artificially made rock-like specimens of similar characteristics. Since the uniaxial compressive strength of transversely isotropic rocks is known to show 'U' form when tested by its angles formed by loading direction and isotropic axis through theoretical and experimental research, this study was to examine the changes of its form under different loading or strain rate loadings.

The specimens of the study were schist from Boryeong area of Korea, cement mortar, and 3D printed materials in form of transversely isotropic behaviors. The cement mortar specimen had been cored from an artificial block which cement mortar had been alternatively layered by two different

mixing ratios; 100:0 and 70:30 of commercial cement mix:sand from Jumunjin area of Korea. Each layer was to be of 10 mm in thickness. Objet30Pro of Stratasys was used for 3D printing, while PMMA material was used for the specimen. Grid modeled plane formed of 1mm thickness and height located every 1 mm was removed from the cylinder to express weak layers every 10 mm. Artificial specimens consisting of 0, 15, 30, 45, 60, 75, 90 degrees of transversely isotropic angles were manufactured. Three loading conditions were used for the test, which were 0.0067 mm/s and 10 mm/s of displacement-controlled loading rate for pressure machine and dynamic condition of free fall for drop weight test machine. Through the uniaxial compression test, the maximum strength was measured with specimens with degree of anisotropy near 0 and 90 degrees when the minimum strength was measured near 45 and 60 degrees. All tests had shown the 'U' form and its anisotropic behavior could be found to take less effect as the loading rate increased. An increase of strength proportion to its loading rate, or strain rate, could only be related to the test results from the same testing method.

By the use of Particle Flow Code 3D (PFC3D) by Itasca, a program to perform discrete element method (DEM) analysis, test results were to be reproduced via numerical simulation. Weak planes were expressed using smooth-joint contacts, weakening the bond among particles. The loading rates in the range of quasi-static and intermediate strain rate was used during the simulation. However, change of loading rate under same micro parameters did not show proper simulation results, requiring further studies. As tests proceeded, the result showed the form of 'U', where the maximum strength was measured near models with degree of anisotropy near 0 and 90 degrees while the minimum strength was measured near 45 and 60 degrees.

Keyword: Intermediate Strain Rate, Transversely Isotropic Rock, Uniaxial Compressive Strength, Boryeong Schist, Cement Mortar, 3D Printing

Student Number: 2019-24903

TABLE OF CONTENTS

List of Tables

List of Figures

Chapter 1. Introduction

Rock is represented by its brittle and strong characteristic. For the excavation of rock, drilling and blasting method or mechanical cutting method is usually used. In drilling and blasting, rock is loaded by a very high speed strain rate. On the while, it was reported that the rock is influenced by intermediate strain rate loading when the rock is excavated by movement or rotation of a mechanical cutting tool (Wicaksana and Jeon, 2020). In mechanical excavation of rock, cutting efficiency is affected by the condition of rock discontinuities, especially by the density and orientation of the discontinuities. On the other hand, the deformation and destructive behavior of rocks vary with changes in the loading speed in which relatively higher strength and lower anisotropic behaviors are known to be expressed at higher loading speeds (Jung and Kim, 2006; Zhang and Zhao, 2014). Most rocks exhibit anisotropic behaviors, and when the discontinuities are distributed parallel to each other, as commonly observed in sedimentary rocks, they have transversely isotropic behaviors. Prior studies were conducted on transversely anisotropic rocks in such ways as finite element analysis, discrete element analysis, uniaxial compression test, triaxial compression test, Brazilian tension test on shale, gneiss, schist, and artificial rocks (Tien et al., 2006; Gholami and Rasouli, 2014; Park and Min, 2018; Wicaksana and Jeon, 2020).

Tien et al. (2006) conducted uniaxial compression test for simulated transversely isotropic rock by mixing cement and kaolinite to examine the destructive behavior under static loading condition as shown in Fig. 1.1. The cases of failure were grouped into two big categories: sliding failure and non-

sliding failure. Brady and Brown (1993) summarized the maximum axial stress in triaxial compression for transversely isotropic rocks as shown in Fig. 1.2 and Fig 1.4. For the theory that was previously proposed by Jaeger (1960), Goodman (1989) proposed Equations (1.1) and (1.2) by organizing the laboratory test data of real transversely isotropic rocks as shown in Fig. 1.3.

$$S_i = S_1 - S_2[\cos 2(\varphi - \varphi_{min,s})]^n \quad (1.1)$$

$$\tan\phi = T_1 - T_2[\cos 2(\varphi - \varphi_{min,\Phi})]^m \quad (1.2)$$

Where, S_1, S_2, T_1, T_2, m, n are constants, φ is angle between the fracture of bedding and the direction of maximum principal stress, ϕ is friction angle, $\varphi_{min,s}$ and $\varphi_{min,\Phi}$ is angle between the fracture of bedding and the direction of maximum principal stress when S_1 and φ is minimum respectively.

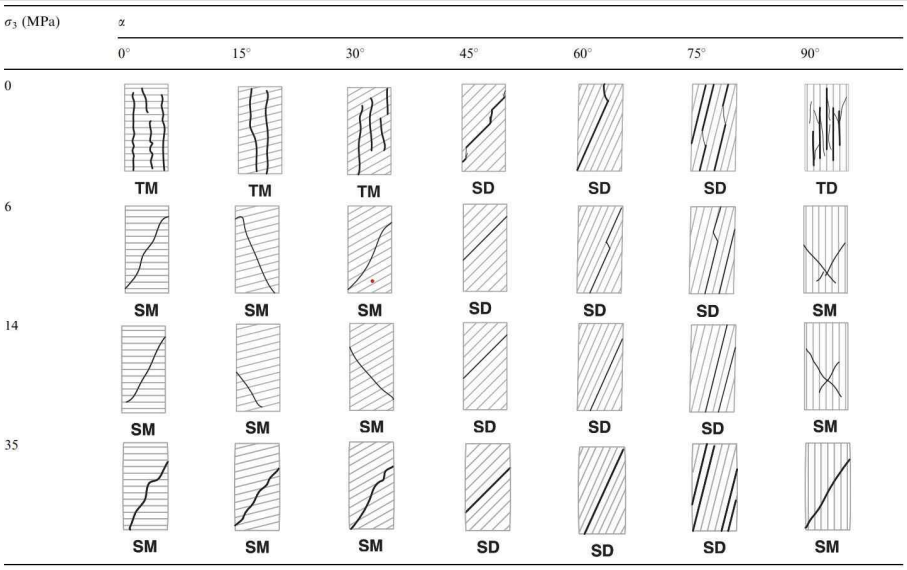

TD: Tensile-split along discontinuities.
TM: Tensile fracture across discontinuities.
SM: Sliding failure across discontinuities.
SD: Sliding failure along discontinuities.

Fig. 1.1 Failure modes of simulated transversely isotropic rock observed in experiments (Tien et al., 2006)

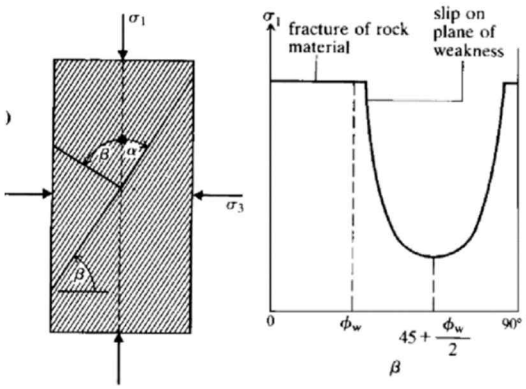

Fig. 1.2 (a) Transversely isotropic specimen in triaxial compression (b) variation of peak strength at constant confining pressure with the angle of inclination of the normal to the plane of weakness to the compression axis (Brady and Brown, 1993)

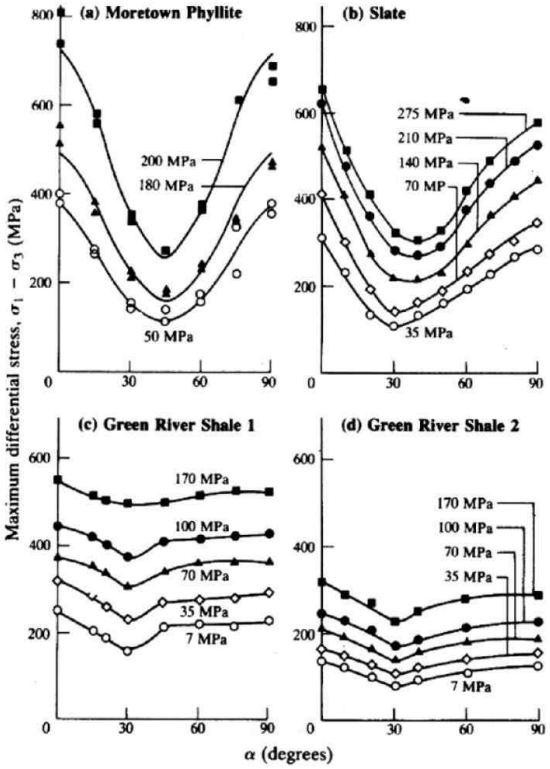

Fig. 1.3 Variation of peak principal stress difference with the angle of inclination of the major principal stress to the plane of weakness, for the confining pressures indicated for (a) a phyllite (after Donath, 1972), (b-d) a slate and two shales (Brady and Brown, 1993)

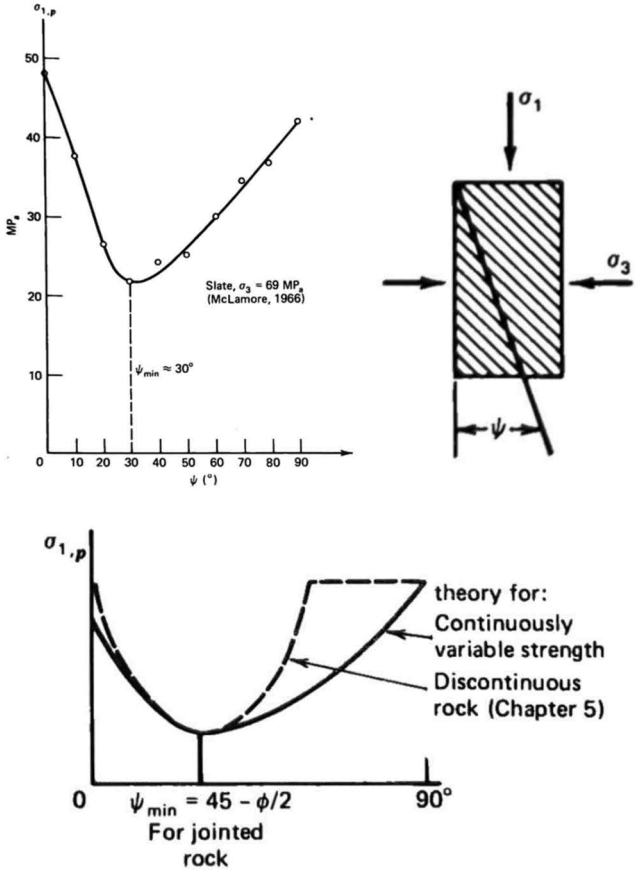

Fig. 1.4 Strength anisotropy in triaxial compression (Goodman, 1989)

In the study of Gholami and Rasouli (2014), slate rock samples from Sardasht Dam in Iran were tested in saturated and dry conditions through uniaxial compression test, triaxial compression test and Brazilian tension test. Especially in uniaxial compression test, regardless of its dry or wet condition, 'U' shaped strength and deformation behavior depending on its degree of anisotropy was confirmed as shown in Fig. 1.5 and Fig. 1.6.

The mechanical behavior of rocks is mostly studied under static loading conditions. In mechanical excavation, rock is subjected to dynamic loading

rather than static loading, in which it is more likely under intermediate strain rate loading. The Split Hopkins Pressure Bar test to examine the behavior of rocks at high strain rates is mainly used for testing rock properties under dynamic load strain loading, and tests on isotropic samples were found to occupy most of them. On the other hand, it was investigated that there are only few dynamic load tests on transversely isotropic rocks. In addition, studies on strength and properties of anisotropic rocks under intermediate strain rate loading for cutting efficiency of mechanical cutting tools for rocks are required. In this study, drop weight testing method was used to test anisotropic rocks under intermediate strain rate condition. Experiments with

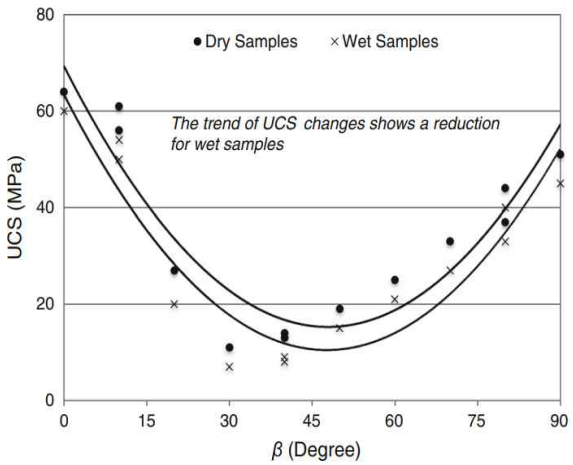

Fig. 1.5 Plot of uniaxial compression test data with respect to the angle of anisotropy β (Gholami and Rasouli, 2014)

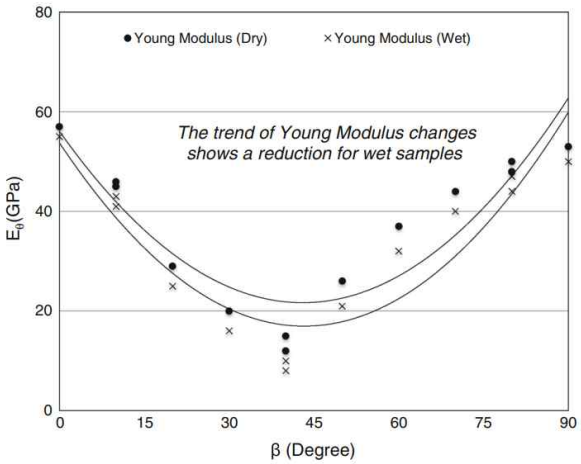

Fig. 1.6 Variation of apparent Young's modulus with respect to anisotropy angle β (Gholami and Rasouli, 2014)

anisotropic rocks require more tests than experiments with isotropic rocks. Due to the nature of rock, it is difficult to obtain numerous specimens with the identical geographical, geological, environmental, and weathering condition. Therefore, the use of artificial samples that can produce large quantities of specimens under equivalent conditions is advantageous (Tien et al., 2006). In this study, in addition to the test for real anisotropic rock, the experiment was repeated using artificial specimens produced with cement mortar and 3D printing material.

It is worth noting that numerical experiment has great benefits when various testing conditions cannot be realized in the real laboratory or field testing. In this study, Itasca's PFC3D (Particle Flow Code 3D), a commercial program that uses a DEM (Discrete Element Method)-based particle bonding model, was used to reproduce the laboratory test results. In the PFC3D model, which describes rock specimens are consisted by particles, the deformation

and fracture behavior of rocks can be studied by applying load to the model. (Cundall, 2001; Potyondy, 2010) Particles are subjected with properties such as normal stiffness, shear stiffness, shear strength etc. It can be effectively used to visualize the analysis results. However, due to the spherical form and bonding between particles, there is a limit to effectively simulate the behavior of discontinuities of rocks such as cracks and joints in PFC. Therefore, the smooth joint model can be successfully used in this case which was developed to have the particles to cross and slide each other as shown in Fig. 1.7 (Mas Ivars et al., 2008, 2011). Since transversely isotropic rocks have the characteristic that their isotropic layers appear alternately, it is effective to simulate it using a smooth joint model, and there are already successful cases of application via studies (Park and Min, 2018).

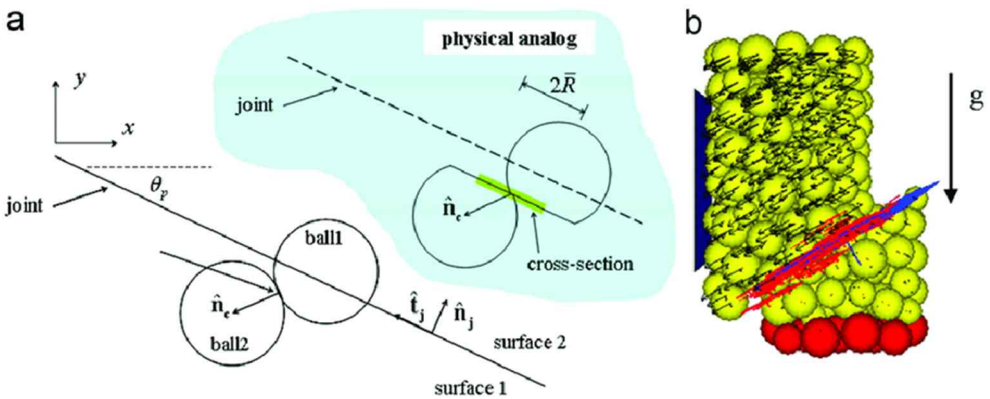

Fig. 1.7 (a) effect of smooth-joint contact (b) 3D specimen with smooth-joint contact model applied (Mas Ivars et al., 2008)

Fig. 1.8 shows the fracturing behavior of Boryeong shale that has transversely isotropic characteristics and its numerical analysis using PFC3D (Park and Min, 2018). Fig. 1.9 shows the stress-strain curve of the actual rock specimen and the PFC3D analysis. Although it is difficult to derive results that quantitatively match the laboratory tests through numerical analysis, it is reported that it is possible to reliably simulate the experimental results (Cundall, 2001; Potyondy, 2010, 2015; Park and Min, 2012, 2018). In this study, the uniaxial compressive strength, fracture behavior, and anisotropic characteristics of transversely isotropic rock and similar artificial rock samples under two static loading rate conditions and intermediate strain rate condition through drop weight test were studied, and they were simulated using PFC3D as well.

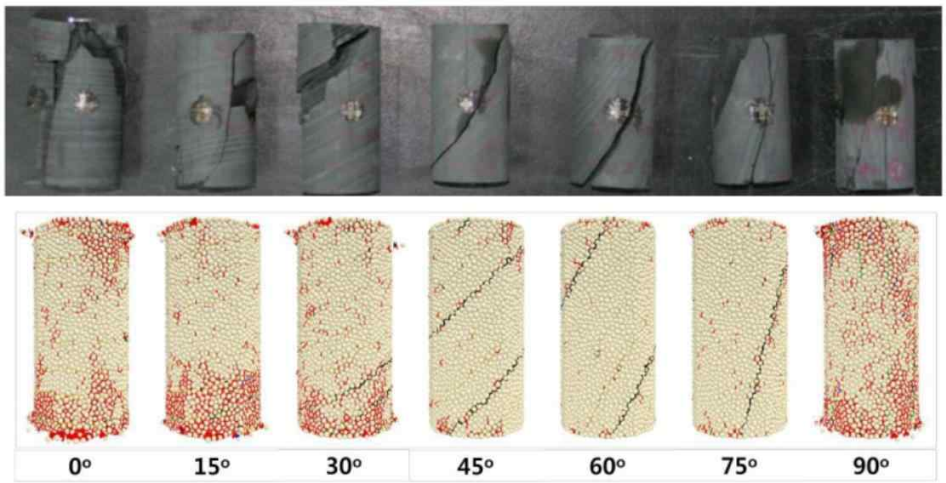

Fig. 1.8 Comparisons of post failure specimens obtained from Boryeong shale and three-dimensional DEM model (Park and Min, 2018).

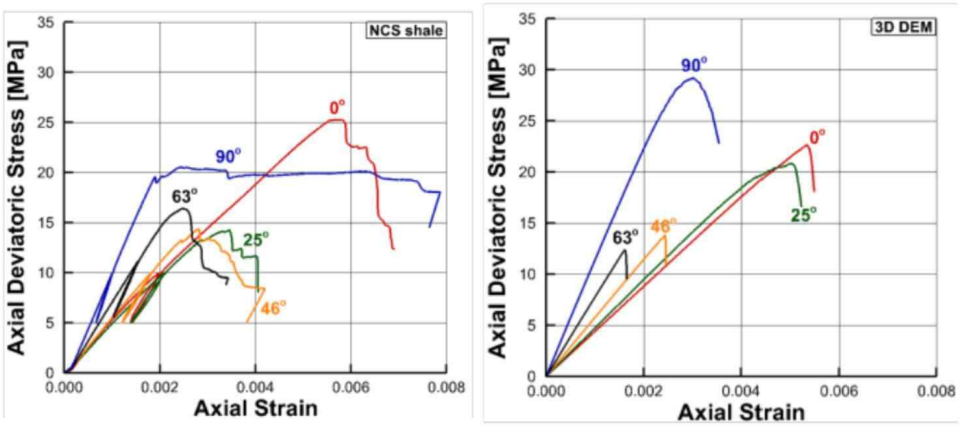

(a) (b)

Fig. 1.9 Comparisons of axial stress-strain curves obtained from (a) NCS (Norwegian Continental Shelf) shale and (b) three-dimensional DEM model (Park and Min, 2018).

Chapter 2. Literature Review

2.1 Static and Dynamic Rock Test

In examining the deformation and fracturing characteristics of a rock, a series of tests that simulates the corresponding static and dynamic load conditions should be carried out in consideration of the cases where the rock is in various loading rate environments. Zhang and Zhao (2014) defined the strain rates that the rock specimen receives under various loading rates by classifying it as in Fig. 2.1 and arranged test methods corresponding to it. Fig. 2.1 indicates that rock testing can be classified into five major types (creep, quasi-static strain rate, intermediate strain rate, high strain rate, and very high strain rate) according to the strain rate. Because the purpose of this study is

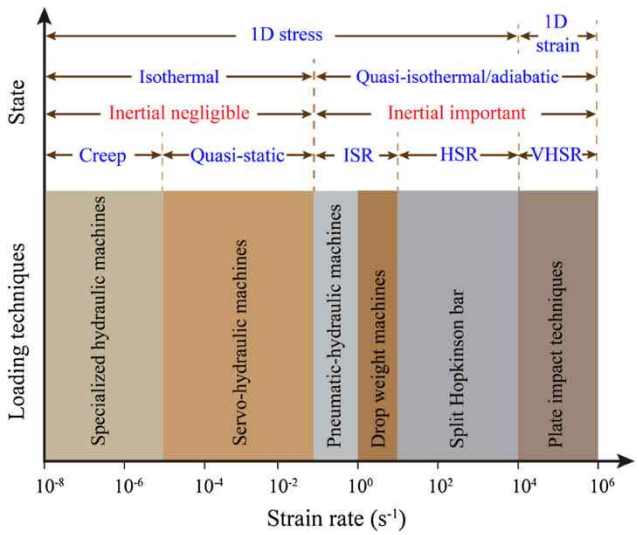

Fig. 2.1 Classification of loading techniques and the state of rock materials over a wide range of strain rates (Zhang and Zhao, 2014)

to examine the difference in rock fracture behavior under static and intermediate strain rate loading conditions, uniaxial compression test and drop weight test were conducted, which are tests of the quasi-static strain rate and the intermediate strain rate between strain rates of $10^{-5}\ s^{-1}$ and $10^{1}\ s^{-1}$. In Wicaksana and Jeon (2020), through experiments using a hydraulic pressure loading control machine and a loading machine using non-explosive powder, the cutting of mechanical excavation equipment had higher strain rate than quasi-static strain rate, but lower than HSR, assuming it to be under the intermediate strain rate. A series of experiments and analysis have been performed to support the theory. Numbers of researchers have used a drop weight machine to study the fracture behavior of rocks under intermediate strain rate loading (Hogan et al., 2012; Reddish et al., 2005; Whittles et al., 2006). The drop weight machine is a simple test device that applies an impact load to a material by dropping a weight. The amount of impact can be derived from the relationship between the weight of the falling weight, the height of the fall, and the time required for impact. (E=mgs; m=weight of drop [kg], g=9.81 m/s^2 , s=drop height[m]). In addition, it is known that the drop weight machine can control the strain rate between $10^{0}\ s^{-1}$ and $10^{1}\ s^{-1}$ by controlling the collision time by placing a deformable material such as a rubber plate on the specimen (Reddish et al., 2005; Zhang and Zhao, 2014; Wicaksana and Jeon, 2020). However, it has been reported that the drop weight machine test is a tool that requires quantitative results through trial and error and repeated experiments because it is not easy to derive quantitative results due to vibration and deformation caused by collision (Zhang and Zhao, 2014).

.

2.2 Discrete Element Method

In the particle bonding model, it is assumed that the material is composed of the bonding of particles, and the bonding between the particles is constrained by the bonding force, so that deformation and destruction are not made without the intervention of an external force (Itasca CG, 2008; Potyondy and Cundall, 2004; Potyondy, 2010, 2015). The bonding of all particles is defined through micro parameters such as normal stiffness, shear stiffness, and shear strength, and it can be set rationally to reproduce the deformation and fracture behavior of the rock (Cundall, 2001). In this study, a transversely isotropic specimen was simulated using PFC3D (Particle Flow Code 3D) analysis software, a commercial program developed by Itasca, and the test results derived from the laboratory test were tried to be reproduced. A particle bonding model with a diameter of 25 mm and a height of 60 mm was modeled to have the same shape and size as the actual lab tested specimen, and discontinuities were included to simulate the transversely isotropic properties. The smooth-joint contact model was used to make the discontinuities similar to the actual rock and artificial specimens, and it was intended to examine whether the results similar to those obtained in the actual test can be reproduced by changing the angle of the soft surface (Mas Ivars et al., 2008, 2011; Park and Min, 2018).

Chapter 3. Test Setup

3.1 Types of Specimen

In this study, rocks and artificial rock samples were used for the purpose of examining the fracture behavior of anisotropic rocks, especially transversely isotropic rocks, subjected to compressive loads under intermediate strain rate loading. For the rock sample, Boryeong schist, which is known to have predominant transverse isotropic properties, was used. For artificial rock samples, cement mortar specimens and 3D printed specimens were used in which the material and thickness were reasonably determined so that the degree of anisotropy was similar to that of the actual rock.

In the production of artificial specimens, the International Society for Rock Mechanics and Rock Engineering (ISRM), the American Society for Testing and Materials (ASTM), and the Korean Society for Rock Mechanics and Rock Engineering (KSRM) and others were cited, and the Suggested Method for Determining the Uniaxial Compressive Strength and Deformability of Rock Materials (ISRM, 1979) was reflected in this study. According to the standard testing method, it is recommended to use a cylindrical specimen with a height/diameter ratio of 2.5 - 3.0 and a diameter of at least 54 mm (NX core) while the diameter is at least 10 times bigger than the biggest particle of the sample. While the standard testing method assumes the loading condition under quasi-static loading, in this study, the intermediate strain rate loading was planned. Test specimens with a smaller diameter of 25 mm was prepared, and the specimen was set to a height of 60

mm to satisfy the standard testing method. Since the particle size of the Boryeong schist sample is known to not exceed 2 mm at most, the diameter of the rock specimen was judged to be appropriate.

Fig. 3.1 shows the shape and manufacturing method of the specimen used in this study. In the case of rock and cement mortar specimens, after obtaining a transversely isotropic sample block, it was cored with the angle between the loading direction and the isotropic plane of the specimen to be 0, 15, 30, 45, 60, 75, and 90 degrees. In the case of 3D printer output samples, each specimen was individually printed.

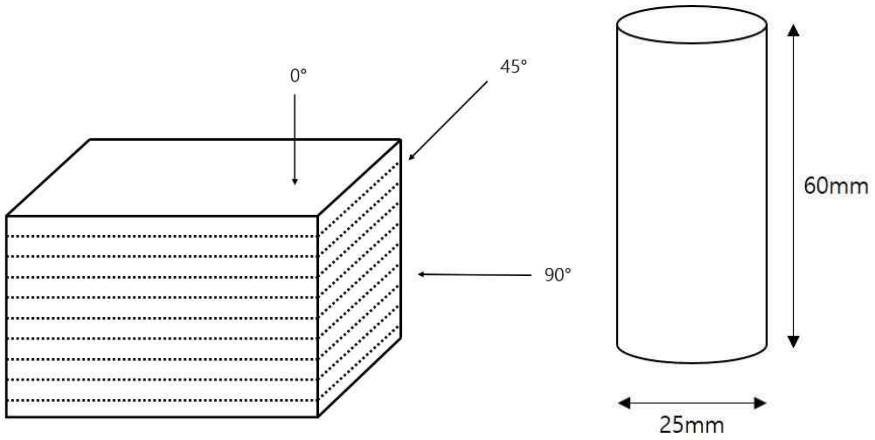

Fig. 3.1 Transversely isotropic specimen: (a) transversely isotropic block, (b) specimen standard

3.1.1 Specimen Mortar Specimen

Cement mortar specimens were manufactured with diameter of 50 mm and height of 100 mm to meet the height/diameter ratio 2 as recommended in KS F 2403 (Concrete Specimens for Strength Test Manufacturing Method) to select the mixing ratio required to produce cement mortar specimens. Uniaxial compression test was performed on three types of cement mortar specimens A, B, and C prepared with different mixing ratios, and a suitable mixing ratio for the experiment was determined based on the results. For the materials used for mixing, cement (Union Corporation, Grout JM) (P), Jumunjin standard sand (S), and water (W) were used, and the mixing ratio is as summarized in Table3.1. For compounds A, B, and C, the strength was adjusted by varying the mixing ratio of cement, and in order to reproduce the transverse isotropic properties, using two types of mixing materials with 10 mm thickness alternately. A and B compounds were decided to be used for this study.

To produce the test specimens, as in Fig. 3.2a, an alternating block of cement mortar A and B by thickness of 10 mm, with 600 mm × 150 mm × 150 mm of size was cured for 14 days. It was then cored with 25 mm of

Table 3.1 Cement mortar mixing ratio

	A	B	C	A-B	A-C
Strength (MPa)	14.73	9.65	9.16	14.6	6.77
Diameter (mm)	50	50	50	24.80	25.00
Height (mm)	100	100	100	60	60
Mixing Ratio (P:S:W)	100:0:20	70:30:20	50:50:20	-	-

diameter and cut approximately in height of 60 mm as shown in Fig. 3.2b. Sets of cement mortar specimens after manufacturing process is as shown in Fig. 3.2c, and the degree of anisotropy of the specimen was set to have 7 variables in total.

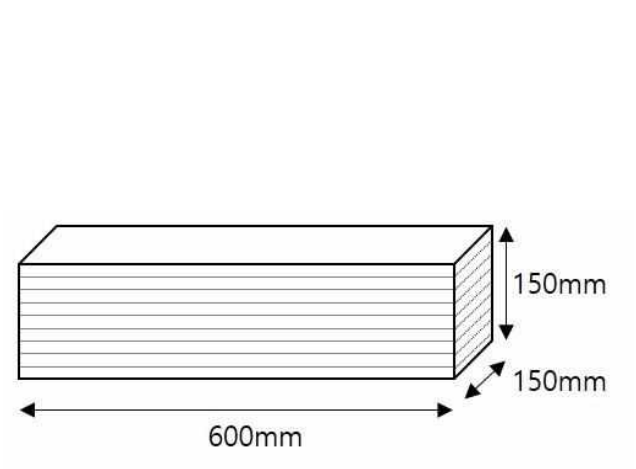

(a)

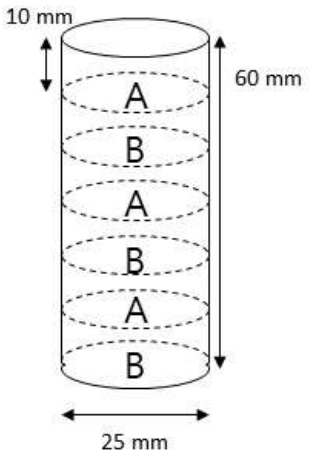

(b)

(c)

Fig. 3.2 Transversely isotropic cement mortar specimen: (a) transversely isotropic cement mortar block, (b) specimen standard, (c) specimen set sample

3.1.2 3D Printed Specimen

3D printing technology has developed rapidly in recent years, making it possible to print using a variety of materials. Common types of 3D printers include the FDM (Fused Deposition Modeling) method, which melts and prints material filaments with a high-temperature head, the SLA (Stereo Lithography Apparatus) method, which prints by shooting laser into a water tank filled with liquid resin, SLS (Selective Laser Sintering) method which shoots lasers to melt and harden powders to form models, and the Polyjet method, in which the material is printed with an inkjet method and hardened with ultraviolet lamp. Materials are also under continuous development in line with the commercialization of 3D printers, from plastics to metals and even food. In this study, considering possible future studies, it was decided that a Polyjet 3D printer that prints PMMA acrylic resin, a transparent material that can visualize internal cracks easily, is to be suitable. Specimens were printed and tested using Stratasys Objet30Pro printer (Table 3.2, Fig. 3.3a), acrylic resin material VeroClear (Table 3.3, Fig. 3.3b), and water-soluble support material (SUP706B). The printed specimen is as shown in

Table 3.2 3D printer specification

Item	Specification
Manufacturer	Stratasys
Model	Objet 30 Pro
Material	Veroclear
Support Material	SUP706B
Layer Thickness	16 ㎛
Resolution	600×600 DPI

Fig. 3.3b, with specimen with 25 mm in diameter and 60 mm in height. Table 3.3 shows the properties of VeroClear material.

(a) (b)

Fig. 3.3 3D printer and specimen: (a) Objet 30 Pro, Stratasys, (b) specimen sample, VeroClear, Stratasys

Table 3.3 3D printer material specification

Properties	Value
Material	Veroclear (PMMA)
Tensile Strength	50 - 65 MPa
Modulus of Elasticity	2 – 3 GPa
Flexural Strength	75 – 110 MPa
Elongation at Break	10 – 25 %

Fig. 3.4 UCS test with 3D printer material (VeroClear): (a) 3D printed specimen before testing, (b) 3D printed specimen after testing

As shown in Fig. 3.4a, an attempt was made to measure the strength of a specimen without anisotropic behavior at room temperature. But as shown in Fig. 3.4b, rock-like brittle fracture behavior was not observed. Meanwhile, among 3D printed materials, it has been reported that acrylic resin (PMMA) based 3D printed specimens exhibit fracturing behaviors similar to that of real rocks in certain environment (very low temperature) (Zhou and Zhu, 2017). To form a very low temperature environment, dry ice which is known to be approximately minus 80°C was fixed around the specimen with aluminum foil. However, though test was conducted as shown in Fig. 3.5, fracturing of brittle behavior did not happen.

Fig. 3.5 UCS test for a VeroClear 3D printed specimen with dry ice attached

An environment capable of maintaining uniform low temperature condition was created by manufacturing aluminum jacketed dry ice chamber module as shown in Fig. 3.6a that can perform uniaxial compression test while continuously exposing the specimen to dry ice to preserve the temperature. The test specimen is placed between the two pressure plates with the jacket made of aluminum designed to prevent the vaporization of dry ice as much as possible, with a window to check the state of failure of the specimen. The test was carried out as shown in Fig. 3.6b, which the brittle fracturing behavior was confirmed through testing (Fig. 3.6c).

3D Printed Specimen (First Trial)

As in Fig. 3.7, the discontinuity was expressed by removing the intersection of a grid with a thickness and spacing of 1 mm at 10 mm intervals from a cylinder with a diameter of 25 mm and a height of 60 mm.

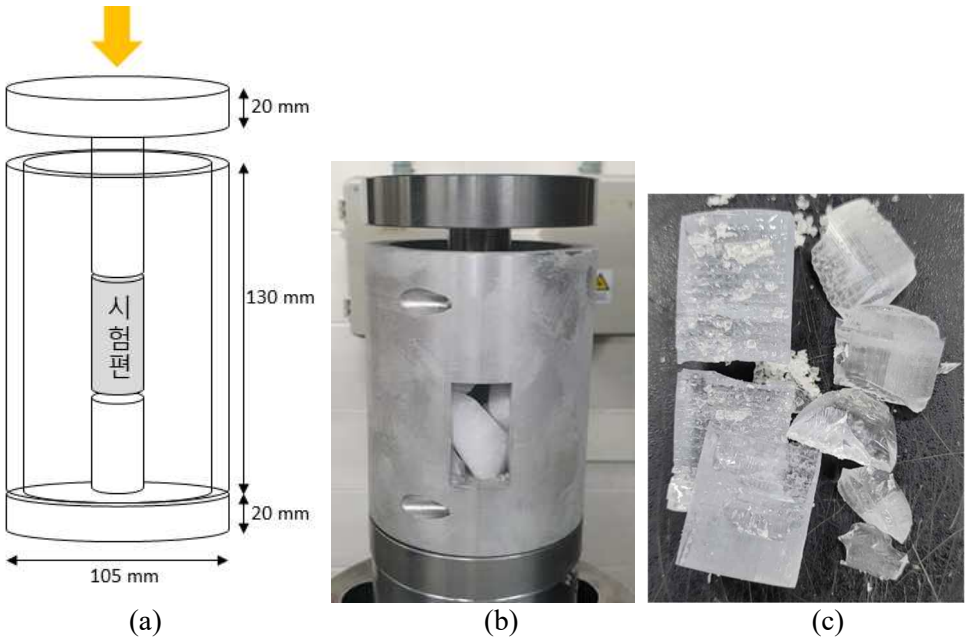

(a) (b) (c)

Fig. 3.6 Dry ice chamber: (a) chamber, (b) chamber under dry ice influence, (c) fractured 3D printer material after test under dry ice condition

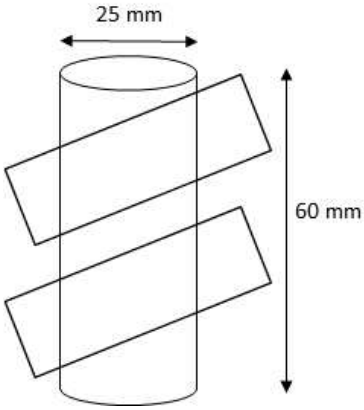

(a)

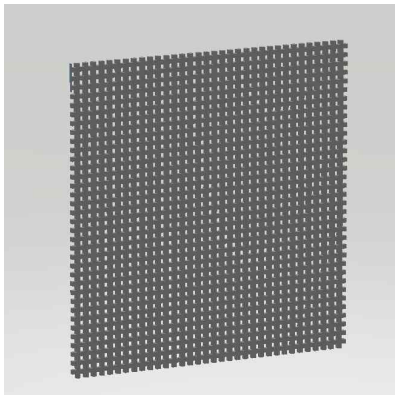

(b)

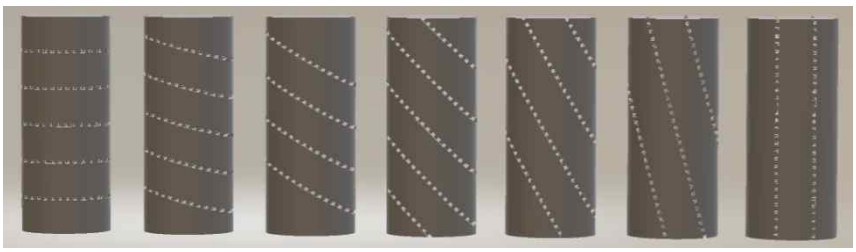

(c)

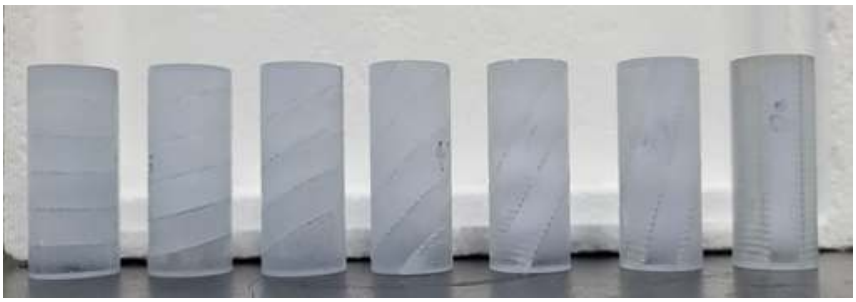

(d)

Fig. 3.7 Transversely isotropic 3D printer specimen: (a) specimen standard, (b) weak layer mesh (c) 3D modeling and (d) printed specimen

3D Printed Specimen (Second Trial)

In the drop weight test, in order to produce a lower strength specimen that meets the test conditions because the primary specimen does not break in the weight free fall test, voids with a size of 1 mm × 1 mm and an interval of 1 mm are created in the cylinder, and then the discontinuity is formed in the same grid pattern as shown in Fig. 3.8.

3.1.3 Rock Specimen

In order to determine the suitability of artificial specimen samples, the same experiment was performed with a specimen formed to be close to 25 mm in diameter and 60 mm in height after coring the Boryeong schist block consisting of the characteristics shown in Table 3.4 (Fig. 3.9).

Fig. 3.8 Transversely isotropic weak 3D printer specimen

Table 3.4 Boryeong schist properties

Properties	Value
UCS	262.67 MPa (α=85°)
Young's Modulus	76 GPa (α=85°)
Density	2.75
Porosity	0.61 %
Elastic Wave (p)	4897 m/s (α=85°)
Elastic Wave (s)	2697 m/s (α=85°)

α = Degree of Anisotropy

(a)

(b)

Fig. 3.9 Transversely isotropic Boryeong Schist: (a) block and (b) specimen

3.2 Types of Test

The test consists of a uniaxial compression test using two strain rate loading condition of a hydraulic loading machine and a test using a drop weight test machine. A total of three strain rate loading conditioned tests are conducted.

3.2.1 Uniaxial Compression

The uniaxial compression test was conducted using the MTS hydraulic loading machine (Fig. 3.10). The test under static loading condition was conducted at a loading rate of 0.0067 mm/s, and the dynamic loading condition was performed at a loading rate of 10 mm/s, which is kwon to be the maximum speed of the testing machine.

The test results were calibrated with an aluminum specimen with a diameter of 25 mm and a height of 60 mm, which is the same size as the specimens used throughout the study. In the case of aluminum 6061 (Unified Numbering System (UNS) designation A96061), it has a Young's modulus of 68 GPa. That is, by subtracting the displacement of aluminum specimen from the displacement of the test result, the displacement of the test equipment corresponding to the load can be confirmed, while the displacement and strain rate of the specimen can be measured by subtracting the displacement of the test equipment from the displacement of the test result (Fig. 3.11). The calibration was carried out and calibrated stress-strain curves such as Fig. 3.12, 3.13, 3.14, and 3.15 can be obtained.

Fig. 3.10 MTS loading machine (Model 816)

Table 3.5 Loading machine information

Item	Specification
Manufacturer	MTS Systems Co.
Model	MTS Model 816.04
Capacity	Up to 2,046 kN
Actuator Displacement	100 mm
Loading Rate	Up to 10mm/s

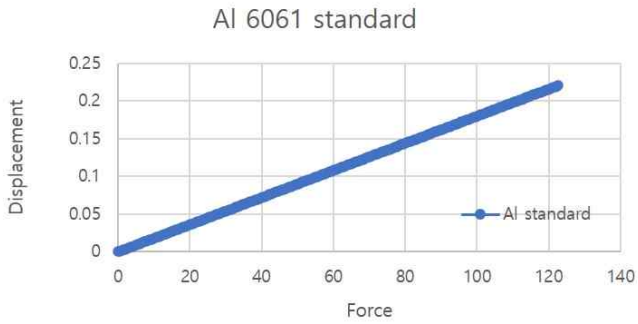

(a)

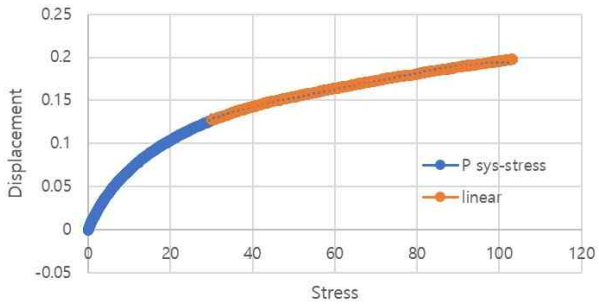

(b)

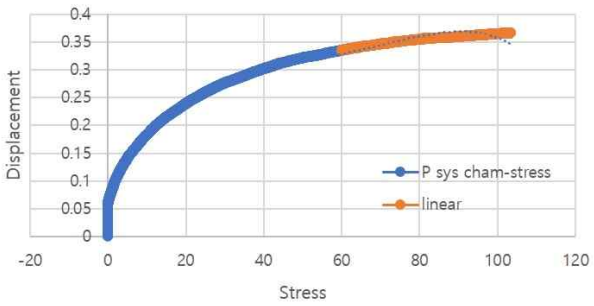

(c)

Fig. 3.11 Loading machine calibration: (a) aluminum 6061, (b) loading machine, (c) loading machine and chamber

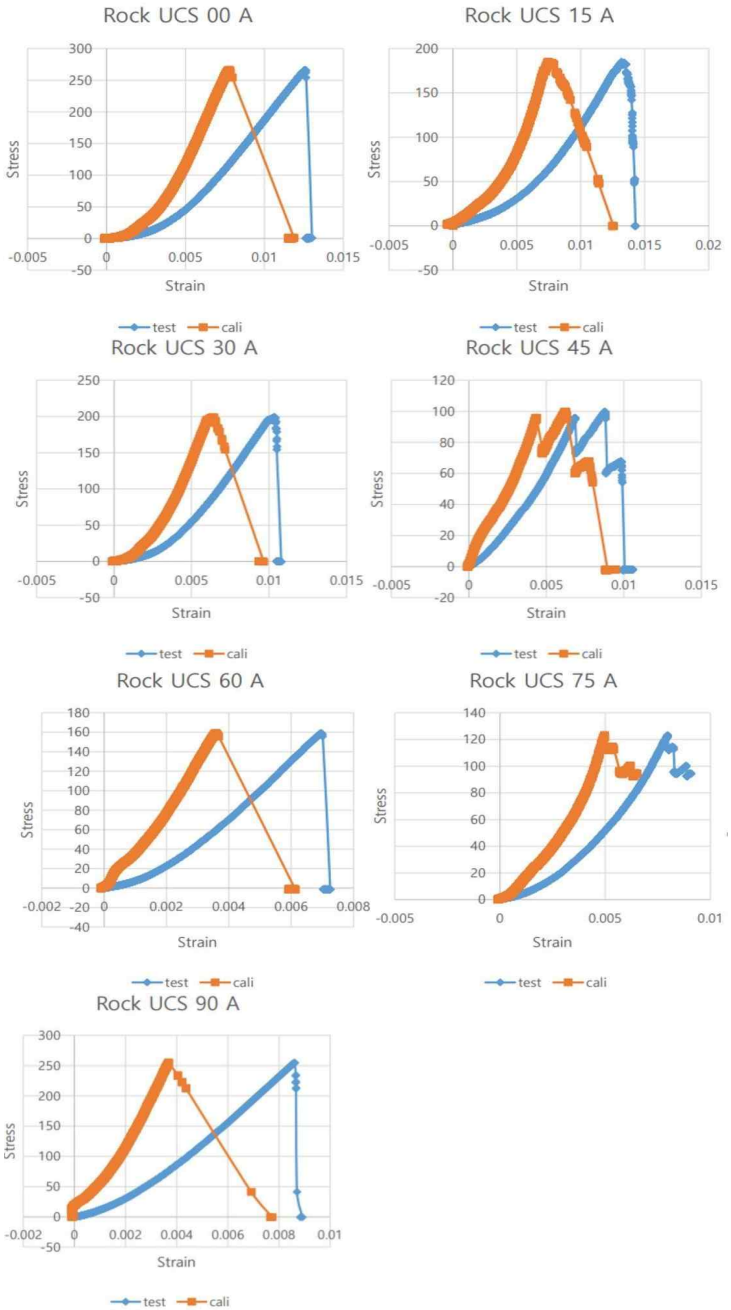

Fig. 3.12 Calibrated Boryeong Schist MTS UCS test result (0.0067 mm/s)

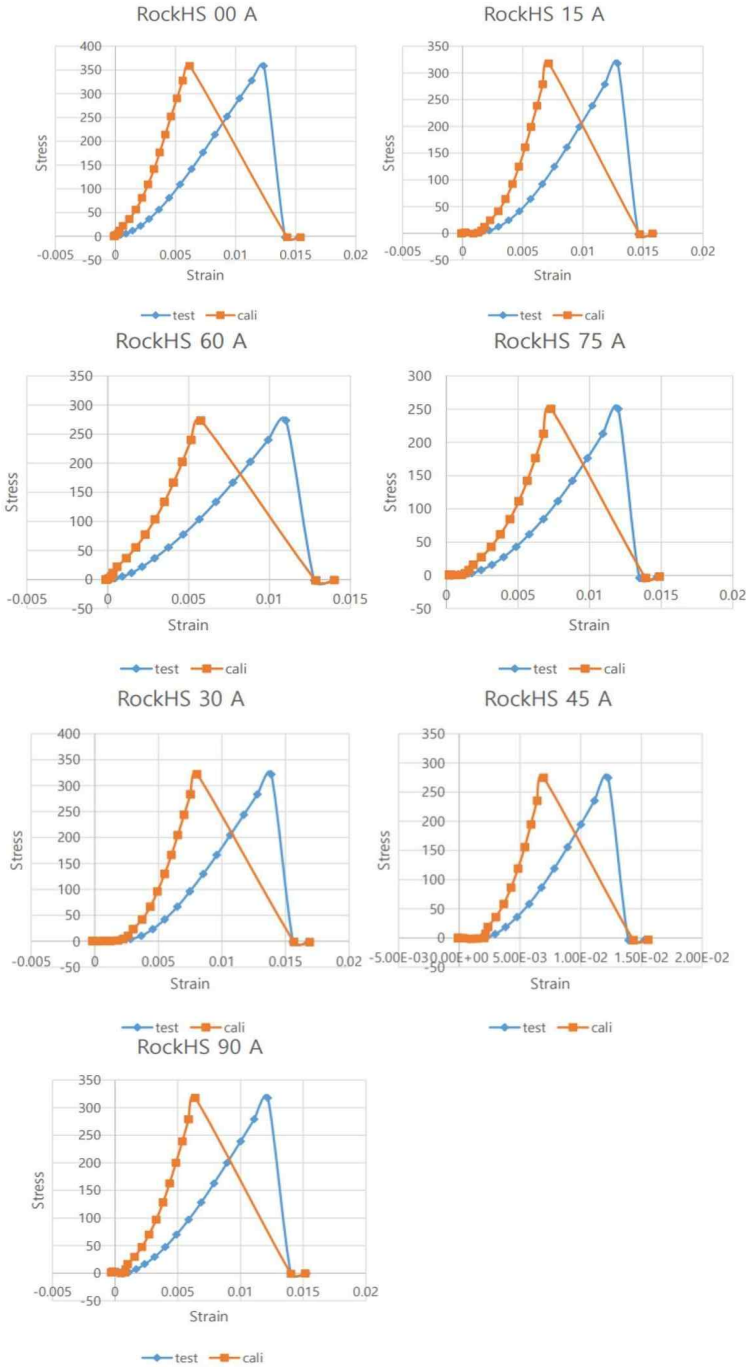

Fig. 3.13 Calibrated Boryeong Schist MTS UCS test result (10 mm/s)

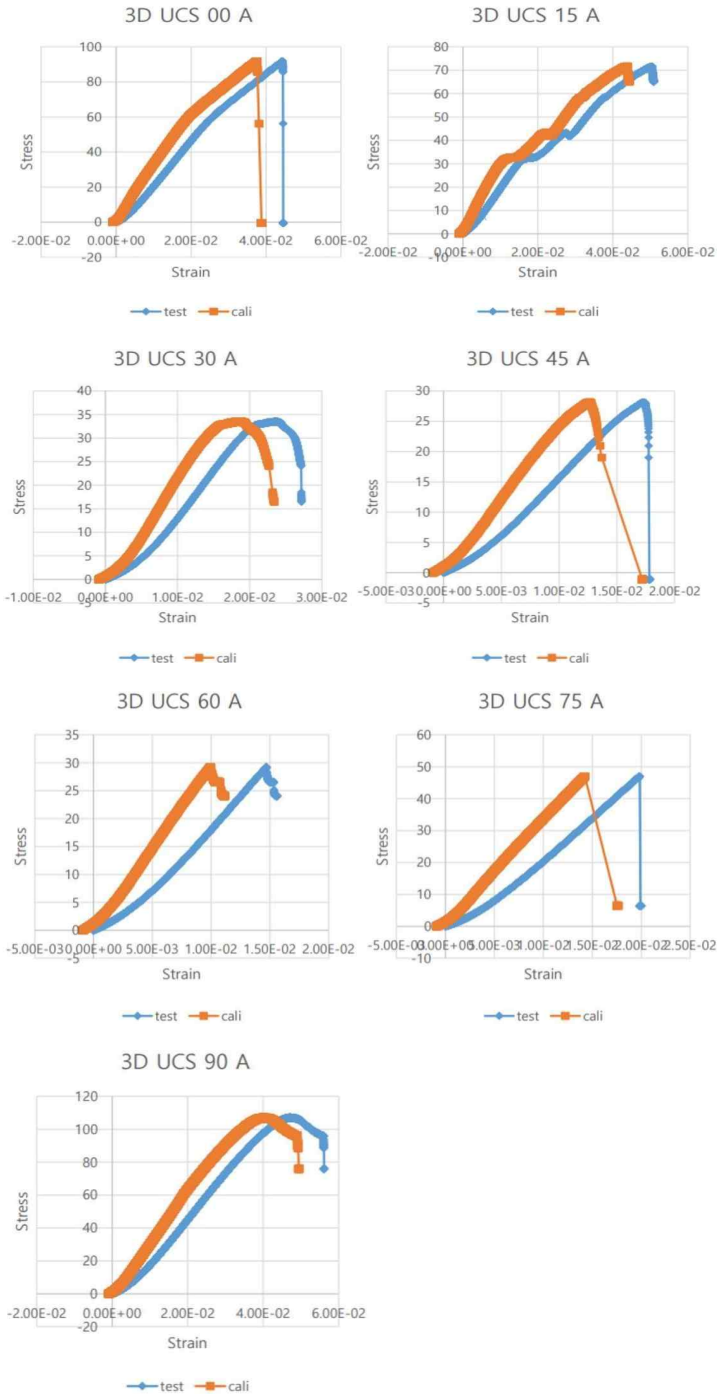

Fig. 3.14 Calibrated frozen 3D printed specimen MTS UCS test result (0.0067 mm/s)

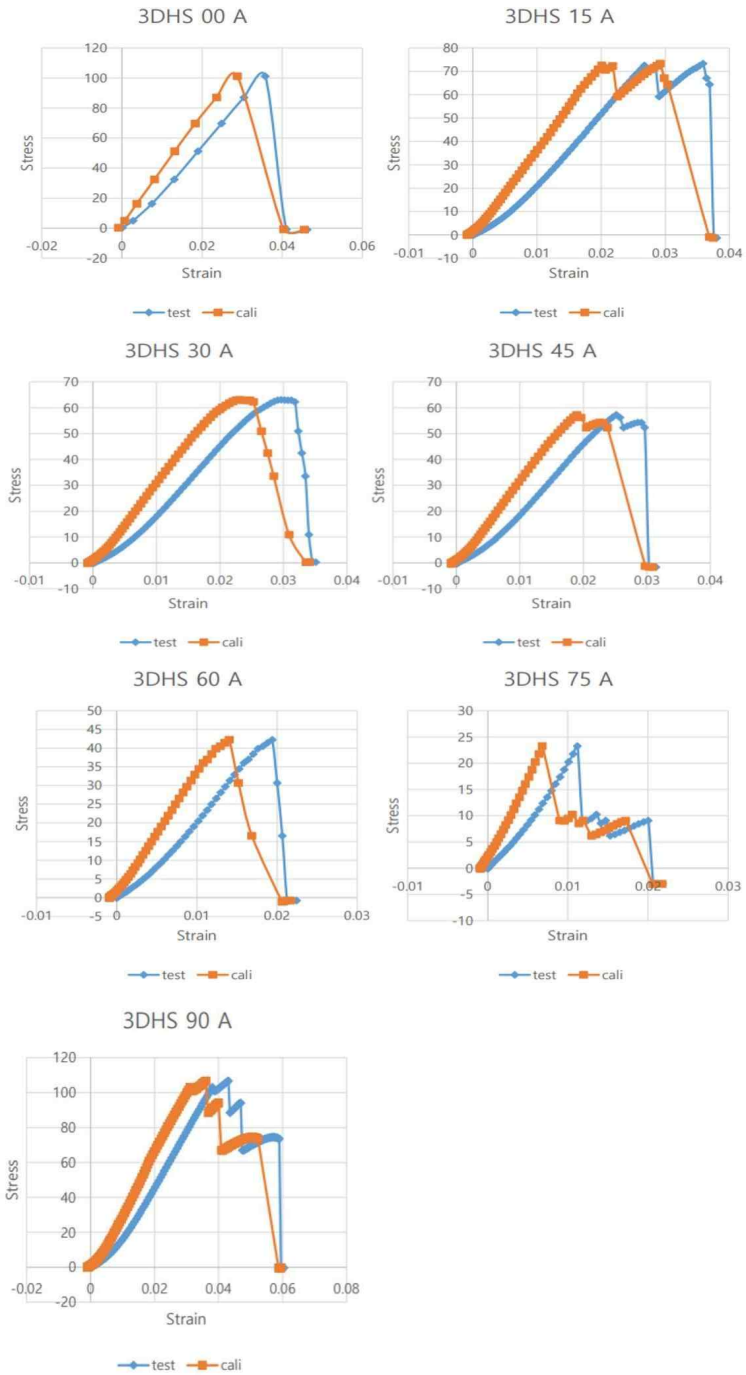

Fig. 3.15 Calibrated frozen 3D printed specimen MTS UCS test result (10 mm/s)

3.2.2 Drop Weight

To test the strength of rocks under intermediate strain rate loading, a drop weight test machine (Table 3.6, Fig. 3.16) was manufactured and used for the test.

Table 3.6 Drop weight machine information

Item	Specification
Maximum drop height	1,700 mm
Elevating Mechanism	Mechanical
Drop Mechanism	Electromagnet
Weight	10 kg

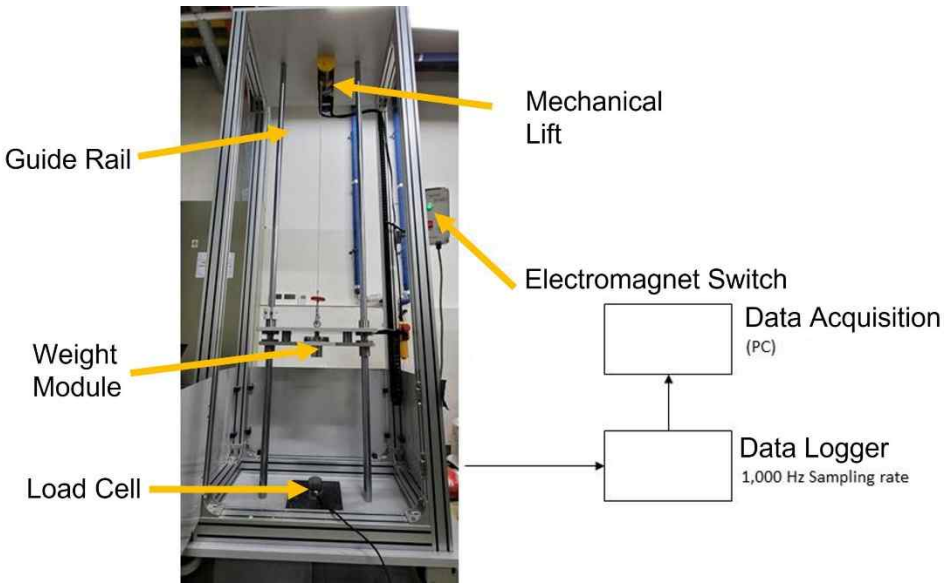

Fig. 3.16 Drop weight test machine system

This is a test method in which a drop module including a 10 kg weight is pulled up mechanically and dropped by blocking the signal to the electromagnet holding on to the drop module. It is a system in which the data logger transmits the signal of the load cell located at the bottom to the PC at the data acquisition rate of 1,000 Hz. The drop axis is fixed with two guide rails for accurate drop impact. For laboratory testing purposes, the maximum drop height was designed to be 1,700 mm. By referring to the UCS strength of each material, the test was conducted several times, and the drop height of failure was selected as shown in Table 3.7.

Table 3.7 Drop height selection based on UCS test

Specimen	Drop Height of Failure (mm)	UCS (MPa)
Cement Mortar	300	8.17 – 29.97
3D Printed	600	5.68 – 19.41
Boryeong Schist	1,400	85.9 – 266.08

Chapter 4. Test Results and Discussion

The strength test of transversely isotropic rock was conducted under three different strain rate loading conditions for three specimens. The summary and results of the test for each specimen are as followed.

4.1 Cement Mortar Specimen

The test results shown in Table 4.1, 4.2, and 4.3 were derived. Although it was the same type of specimen, there was a difference in the absolute value of the strength depending on the testing method. Therefore, the deviation of the maximum and minimum values of strength was measured using the ratio of the maximum and minimum values.

4.1.1 Static Loading Test

The results of the strength of the cement mortar specimen tested under static loading condition via loading machine are as follows.

Table 4.1 Static test results of cement mortar specimen

Loading machine static CM								
Angle		0	15	30	45	60	75	90
UCS (MPa)	Min	13.15	13.67	14.32	8.17	8.19	10.76	12.68
	Max	20.05	22.03	19.25	15.7	13.43	17.56	29.97
	Mean	17.05	17.78	16.35	12.58	10.97	13.52	20.96

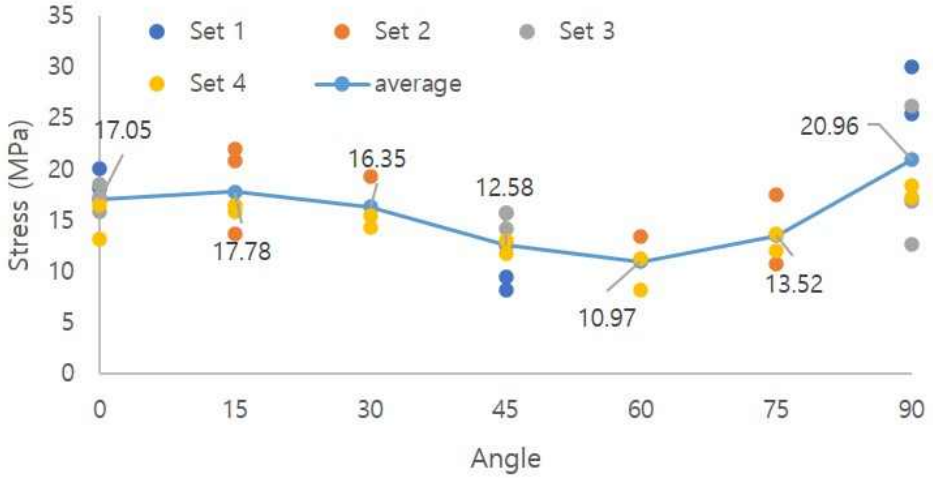

Fig. 4.1 Cement mortar UCS test results (0.0067mm/s)

Uniaxial compression test under static strain rate loading was performed with 4 sets of cement mortar specimens. When the results were averaged, the minimum strength value of 10.97 MPa was measured at the 60° specimen, and the maximum strength value of 20.96 MPa was measured at the 90° specimen (Fig. 4.1).

4.1.2 Dynamic Loading Test

The results of the strength of the cement mortar specimen tested under static loading condition via loading machine are as follows.

Machine dynamic load test was performed with 3sets of cement mortar specimens. When the results were averaged, the minimum strength value of 52.2 MPa was measured at the 60° specimen, and the maximum strength value of 63.42 MPa was measured at the 15° specimen. When calculated as

Table 4.2 Dynamic test results of cement mortar specimen

Angle		0	15	30	45	60	75	90
UCS (MPa)	Min	54.77	62	54.16	53.43	34.73	42.77	60.45
	Max	64.75	64.58	65.82	62.2	67.98	65.91	66.11
	Mean	59.92	63.52	60.83	58.19	52.2	55.8	62.97

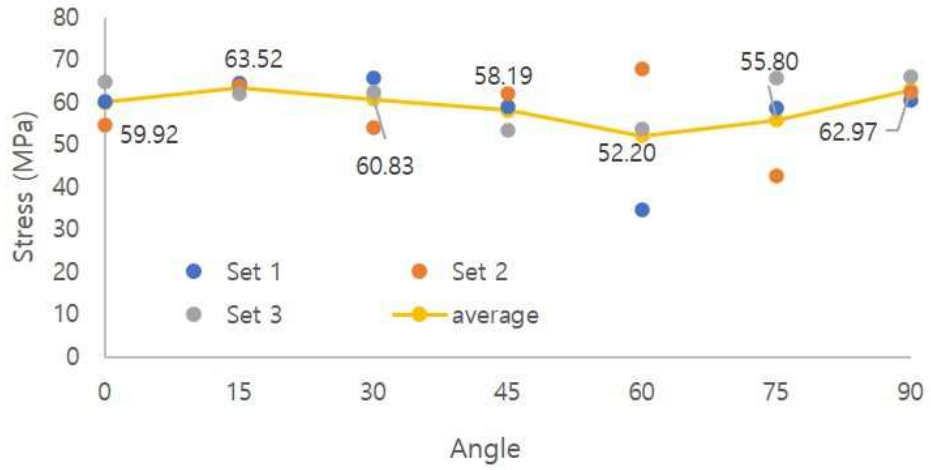

Fig. 4.2 Cement mortar UCS test results (10mm/s)

the ratio of the maximum and minimum values, the machine dynamic load test on cement mortar was 56.56% higher than the static load test. The overall average strength of the static load test was 15.6 MPa, and the average strength of the dynamic load test was 59.06 MPa, which increased by 278.59%. As a result, it was confirmed that the difference between the maximum and minimum values of strength occurred as the loading rate and strain rate of the machine increased (Fig. 4.2).

4.1.3 Drop Weight Test

Table 4.3 shows the strength results of the dynamic load test of cement mortar specimens tested with a drop weight tester.

Table 4.3 Drop weight test results of cement mortar specimen

Angle		0	15	30	45	60	75	90
UCS (MPa)	Min	20.25	15.78	18.88	15.2	7.35	7.3	13.81
	Max	20.25	15.78	33.22	22.9	27.02	28.68	22.01
	Mean	20.25	15.78	26.05	19.05	17.185	17.99	17.91

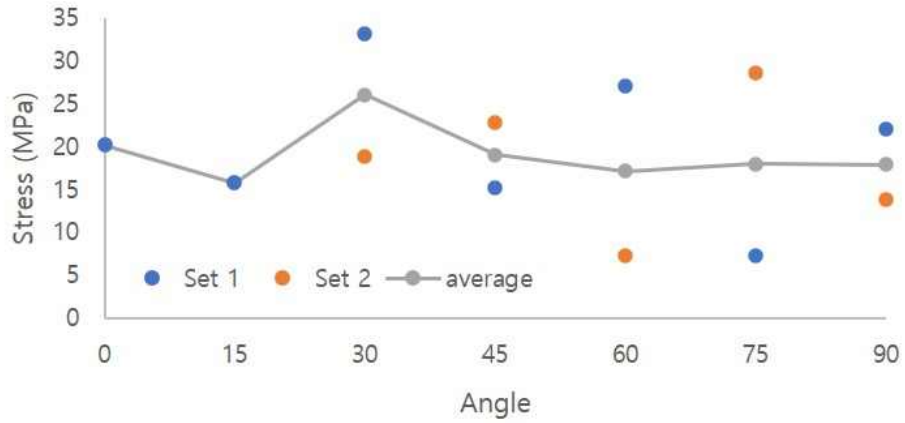

Fig. 4.3 Cement mortar test results, drop weight machine

Drop weight dynamic load test was performed with 2 sets of cement mortar specimens. When the results were averaged, the minimum value of strength of 15.78 MPa was measured in the specimen at 15°, and the maximum value of 26.05 MPa in strength was measured in the specimen at 30°. However, the minimum value of actual strength was measured at 60° and 75° specimens, and when calculated as the ratio of the maximum value and the minimum value, drop weight test result was 15.76% higher than the static machine load test result. The overall average strength of the static load test was 15.6 MPa, and the average strength of the drop weight test was 19.17 MPa, which increased by 22.88%. For the same specimen, it was confirmed that the deviation of the maximum and minimum values of strength decreased as the loading rate and strain rate increased (Fig. 4.3).

The strength of the cement mortar specimens for the machine static load, machine dynamic load, and drop weight test is as follows.

Table 4.4 Cement mortar specimen test results

	Highest UCS (MPa)	Lowest UCS (MPa)	Highest/Lowest
Machine Static	20.96	10.97	1.91
Machine Dynamic	63.52	52.20	1.22
Drop Weight	26.05	15.78	1.65

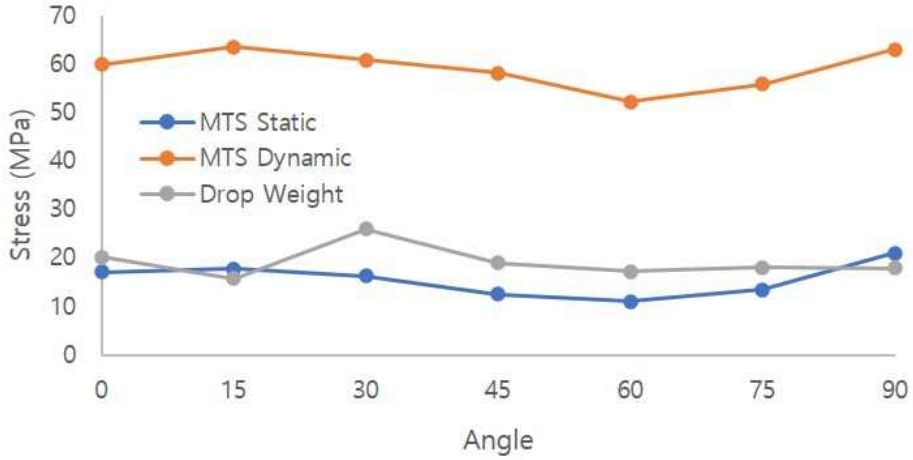

Fig. 4.4 Cement mortar test results

It was confirmed that the expression of anisotropic properties decreased with the increase of the strain rate loading, but no increase in the strength value regardless of the test environment was confirmed (Fig. 4.4).

4.2 3D Printed Specimen

The test results shown in Tables 4.5, 4.6, and 4.7 were derived. The second trial specimen with lower strength was used for the drop weight test. Since the absolute strength of the two specimens do not meet the same standard, the difference between the maximum and minimum values was measured using the ratio of the maximum and minimum values.

4.2.1 Static Loading Test

Brittle fracturing was not observed in room temperature static load test.

Strength result of the 3D printered specimen in a low temperature and static loading state tested with loading machine is as follows.

Machine static load test was performed with 2 sets of 3D print ed specimens. When the results were averaged, the minimum value of strength was measured at the 45° specimen and the maximum strength was measured at the 90° specimen (Fig. 4.5). Although only two sets of tests were performed, there was hardly any difference in strength.

Table 4.5 Static test results of 3D printed specimen

Angle		0	15	30	45	60	75	90
UCS (MPa)	Min	88.07	69.1	33.53	19.84	29.23	47	107.01
	Max	91.8	71.65	35.92	28.15	31.07	48.16	113.63
	Mean	89.94	70.38	34.73	23.99	30.15	47.58	110.32

Fig. 4.5 3D printed specimen UCS test results, MTS (0.0067 mm/s)

4.2.2 Dynamic Loading Test

The results of the dynamic machine load test of the 3D printed specimen tested with a loading machine are as follows (Table 4.6).

Machine dynamic load test was performed with 2 sets of 3D printed specimens under dry ice temperature condition. When the results were averaged, the minimum value of strength was measured in the specimen at 75° and the maximum value in strength was measured in the specimen at 90°. When calculated as the ratio of the maximum and minimum values, the

Table 4.6 Dynamic test results of 3D printed specimen

Angle		0	15	30	45	60	75	90
UCS (MPa)	Min	98.76	73.28	63.07	31.9	41.15	23.29	106.67
	Max	101.21	97.74	77.23	57.27	42.21	35.3	120.78
	Mean	99.99	85.51	70.15	44.59	41.68	29.29	113.73

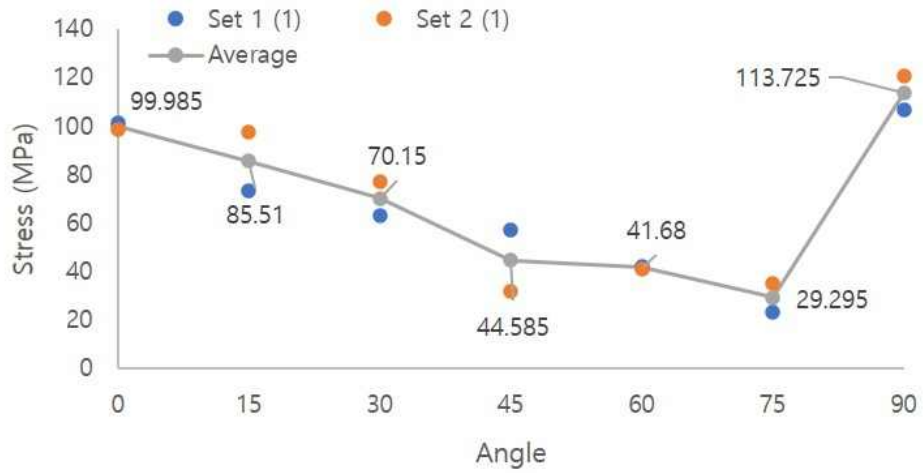

Fig. 4.6 3D printed specimen UCS test results, (10 mm/s)

strength of the dynamic load test using loading machine was 10.58% higher than that of the static load test. When calculated as the ratio of the maximum and minimum values, the strength of the dynamic load test using the loading machine was 10.58% higher than that of the static load test. As a result, it was confirmed that the deviation of the maximum and minimum values of strength decreased as the loading rate and strain rate of the loading machine increased (Fig. 4.6).

4.2.3 Drop Weight Test

In the drop weight test at room temperature, as shown in (Fig. 4.7), the 45 and 60 degree specimens slip fractured and showed no brittle fracturing behavior, causing the measured strength very small.

For the purpose of brittle fracturing behavior, new specimen had been modeled. The results of the drop weight test of the second trial 3D printed specimens are as follows.

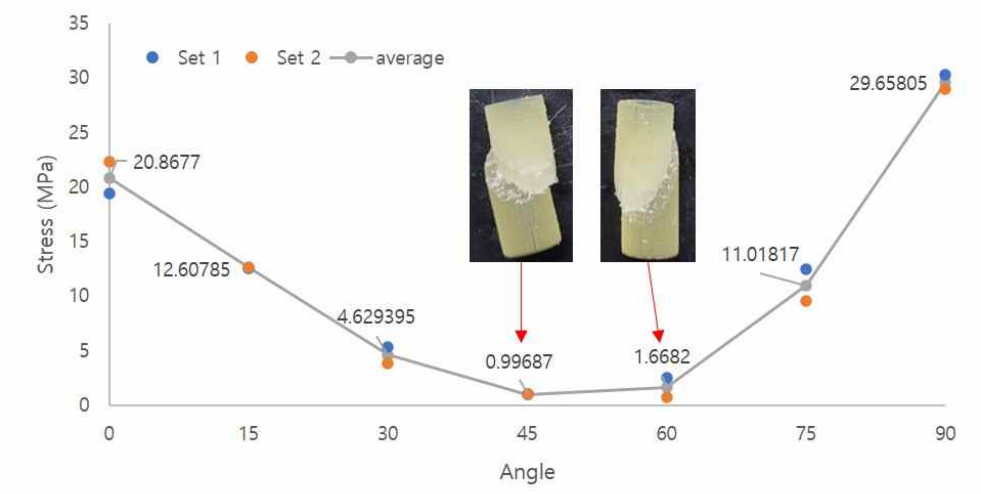

Fig. 4.7 3D printed specimen test results, drop weight machine

Table 4.7 Drop weight test results of 3D printed specimen

Angle	0	15	30	45	60	75	90
UCS (MPa)	34.78	32.21	28.32	22.3	19.85	26.3	37.19

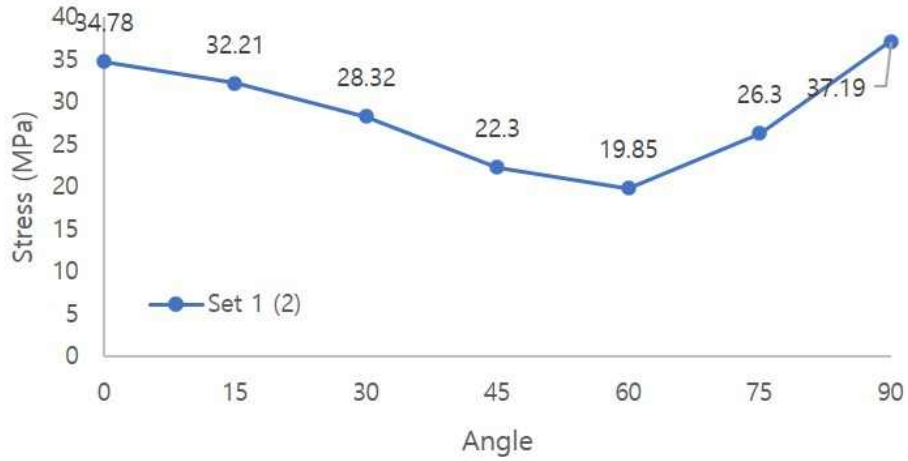

Fig. 4.8 Frozen 3D printed specimen test results, drop weight machine

Drop weight test was performed with one set of second trial 3D printed specimens. The minimum value of strength was measured in the test at 60°, and the maximum value in strength was measured in the test at 90°, confirming the same U-shaped result as the test performed with a loading machine. When calculated as the ratio of the maximum value and the minimum value, the drop weight test result was 145.99% higher than the static load test result using a loading machine. The overall average strength of the static load test using a loading machine was 58.15 MPa, and the average strength of the drop weight test was 28.71 MPa, which decreased by 50.63%. For the same specimen, it was confirmed that the deviation of the ratio of the

maximum and minimum values of strength according to the increase of the loading rate decreased, while the average strength decreased (Fig. 4.8). The strength of the 3D printed specimen for machine static load test, machine dynamic load test, and drop weight test is as follows (Table 4.8).

Table 4.8 3D printed specimen test results

	UCS_{max} (MPa)	UCS_{min} (MPa)	Max/Min
SH machine Static	110.32	23.99	4.60
SH machine Dynamic	113.73	27.36	4.16
Drop Weight	37.19	19.85	1.87

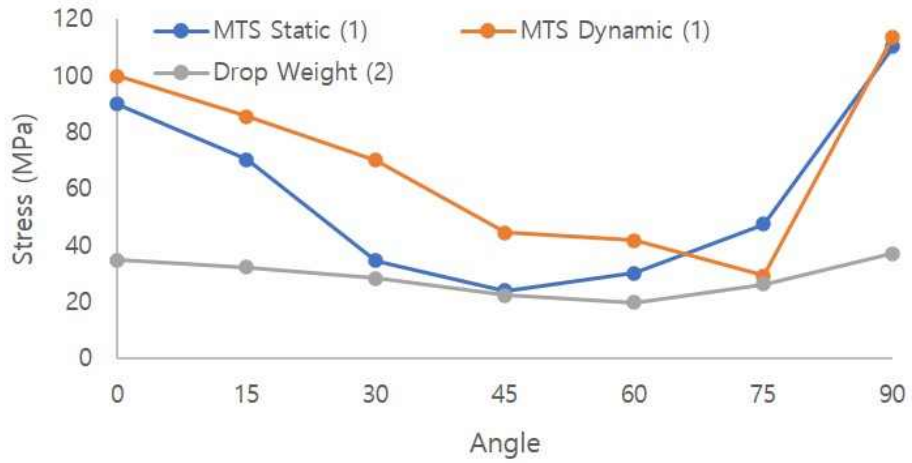

Fig. 4.9 Frozen 3D printed specimen test results

It was confirmed that the expression of anisotropic properties decreased as the loading rate and strain rate increased, but no increase in strength was confirmed (Fig. 4.9).

4.3 Rock Specimen

The test results shown in Table 4.9, 4.10, and 4.11 were derived. Since the strength of the specimen is not the same according to the test environment, the deviation of the maximum and minimum values of strength was measured using the ratio of the maximum and minimum values.

4.3.1 Static Loading Test

The static load strength results of the rock specimen tested with the loading machine are as follows.

Table 4.9 Static test results of Boryeong schist specimen

Angle		0	15	30	45	55	70	84
UCS (MPa)	Min	201.26	183.8	161.87	85.9	158.96	123.25	254.91
	Max	266.08	230.14	198.65	95.76	216.77	175.35	262.67
	Mean	233.67	206.97	180.26	90.83	187.87	149.30	258.79

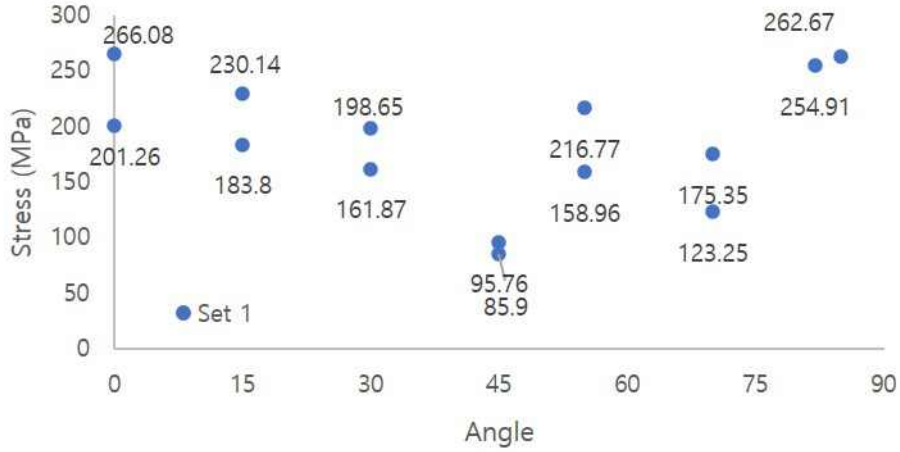

Fig. 4.10 Boryeong schist specimen UCS test results, MTS (0.0067mm/s)

Static uniaxial compression test was performed with two sets of rock specimens using the loading machine. When the results were averaged, the minimum value of strength was measured in the specimen at 45° and the maximum value in strength was measured in the specimen at approximately 85° (Fig. 4.10).

4.3.2 Dynamic Loading Test

The results of the dynamic loading test of the rock specimen tested with a loading machine are as follows.

Table 4.10 Dynamic test results of Boryeong schist specimen

Angle	0	8	15	18	25	30	43
UCS (MPa)	275.10	358.56	93.32	317.85	321.96	224.16	274.68
Angle	45	60	63	72	75	85	90
UCS (MPa)	106.11	244.52	273.28	250.50	299.75	317.49	325.32

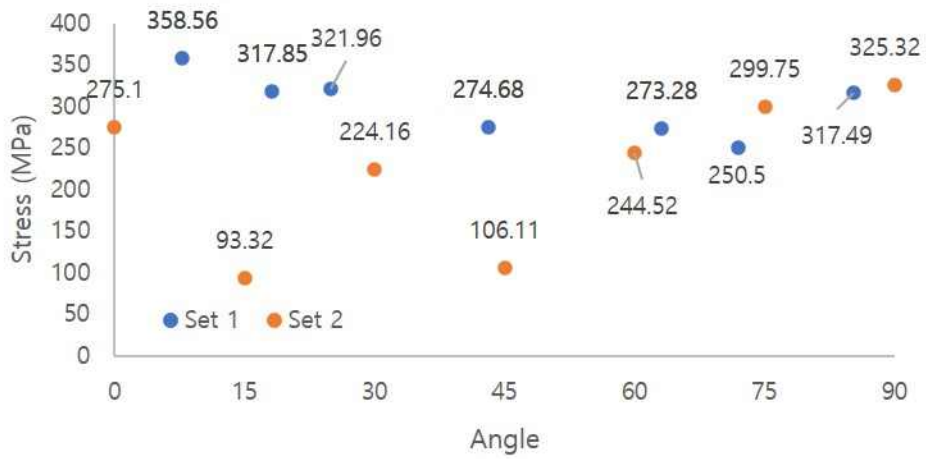

Fig. 4.11 Boryeong schist specimen UCS test results, MTS (10mm/s)

Dynamic loading test was performed with two sets of rock specimens via loading machine. The minimum value of strength was measured in the specimen at 15°, and the maximum value in strength was measured in the specimen at approximately 8°. When ratio of the maximum and minimum value is calculated, the machine static load test result was 30.41% higher than the machine dynamic load test result. The overall average strength of the machine static load test was 186.81 MPa, and the average strength of the machine dynamic load test was 263.04 MPa, which increased by 40.81%. As

a result, it was confirmed that the difference between the maximum and minimum values of strength occurred as the loading rate and strain rate of the loader increased (Fig. 4.11).

4.3.3 Drop Weight Test

The results of the dynamic load test of the 3D printed specimen tested with the drop weight machine are as follows.

Table 4.11 Drop weight test results of Boryeong schist specimen

Angle		0	15	30	45	60	75	90
UCS (MPa)	Min	87.32	71.72	132.65	66.16	54.61	133.74	108.81
	Max	166.13	152.87	135.09	87.98	128.03	149.18	118.85
	Mean	126.73	112.30	133.87	77.07	91.32	141.46	113.83

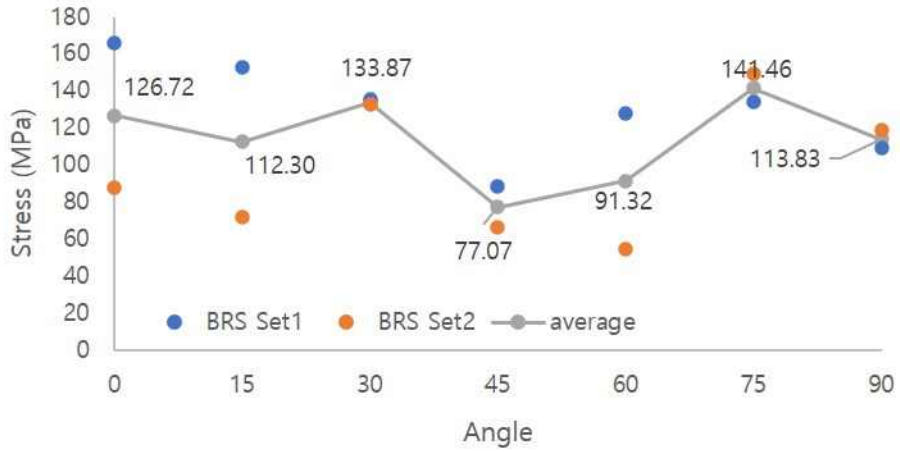

Fig. 4.12 Boryeong schist specimen test results, drop weight machine

Table 4.12 Boryeong schist specimen test results

	UCS_{max} (MPa)	UCS_{min} (MPa)	Max/Min
Machine Static	268.96	136.28	1.93
Machine Dynamic	333.71	224.79	1.48
Drop Weight	136.54	74.34	1.84

The drop weight test was conducted with two sets of rock specimens. The minimum value of strength was measured at the 60° specimen, and the maximum strength was measured at the 0° specimen. When the ratio of the maximum value and the minimum value is calculated, the machine static load test result was 4.89% higher than the drop weight test result. The overall average strength of the machine static load test was 186.81 MPa, and the average strength of the drop weight test was 113.80 MPa, which decreased by 39.08%. For the same specimen, it was confirmed that the difference between the maximum and minimum values of strength occurred as the loading rate and strain rate increased, while the average strength decreased (Fig. 4.12).

Chapter 5. Discrete Element Method

5.1 Commercial Program and Smooth-Joint Model Application

It has been known that the particle flow code (PFC) is suitable for expressing the dynamic behavior of rocks using 2D and 3D (Cundall 2001; Chiu et al., 2013; Yao et al, 2019; Potyondy, 2010, 2015). Through DEM which Smooth-Joint is applied, it can be seen that the numerical model generally simulates the mechanical anisotropy according to the relative inclination of the discontinuity (Mas Ivars et al., 2008, 2011; Park and Min, 2018).

5.2 Modeling and Micro-Parameter Setting

The numerical analysis model (Table 5.1), which mimics the transversely isotropic rock used in this study, is a smooth-joint contact model in the uniaxial compression test code provided as an example. As shown in Fig. 5.1, the test specimen used for the laboratory experiment is reproduced in the same size and simulated through PFC3D (Park and Min, 2018).

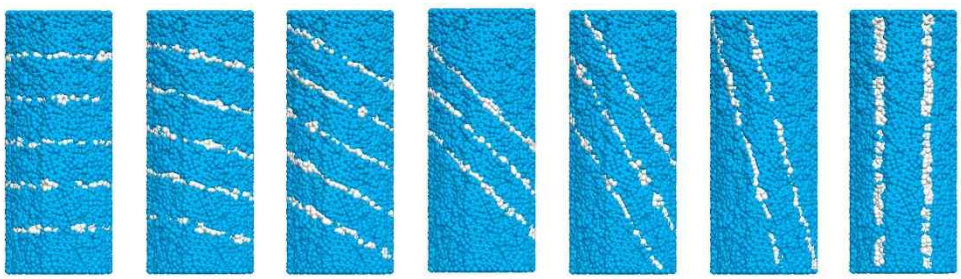

Fig. 5.1 Transversely isotropic PFC model

Table 5.1 Micro-parameter for PFC modeling

Micro-parameter		3D DEM
Particle	Paticle density [kg/m^3]	2,650
	Minimum particle size, D_{min} [mm]	0.6
	Particle size ratio, D_{max}/D_{min} [mm]	1.66
	Total number of particles (cylinder)	10,589
Parallel-bonded model	Radius multiplier	1
	Effective modulus, E_{pbm} [GPa]	61
	Stiffness ratio, K_{pbm}	0.2
	Tensile strength, $\sigma_{t,pbm}$ [MPa]	57
	Cohesion, C_{pbm} [MPa]	70
	Friction angle, ϕ_{pbm} [°]	40
Smooth-joint contact model (weak plane)	Normal stiffness, $k_{n,sj}$ [GPa/m]	7,460
	Shear Stiffness, $k_{s,sj}$ [GPa/m]	1,660
	Tensile strenth, $\sigma_{t,sj}$ [MPa]	5
	Cohesion, C_{sj} [MPa]	20
	Friction angle, ϕ_{sj} [°]	20
	Dilation angle, ψ_{sj} [°]	0
	Average spacing between layers	10

5.3 Results

For the numerical simulation analysis of the uniaxial compression test, it has been tested in two conditions of loading rate of 0.15 mm/s and 0.0015 mm/s while micro parameters were same. The particle behavior, strength and

stress-strain curves of the analysis model were derived as followed (Fig. 5.2, 5.3, Table 5.2).

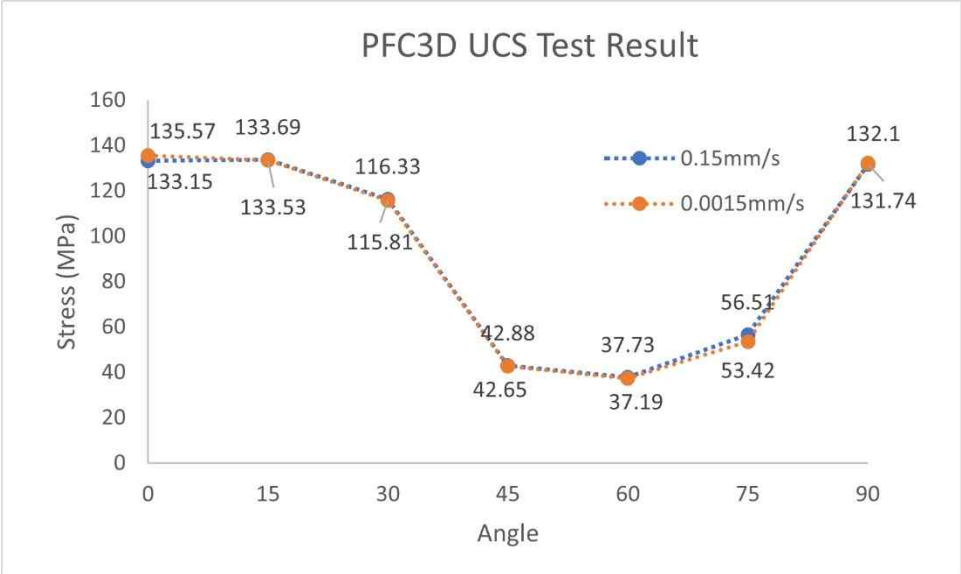

(a)

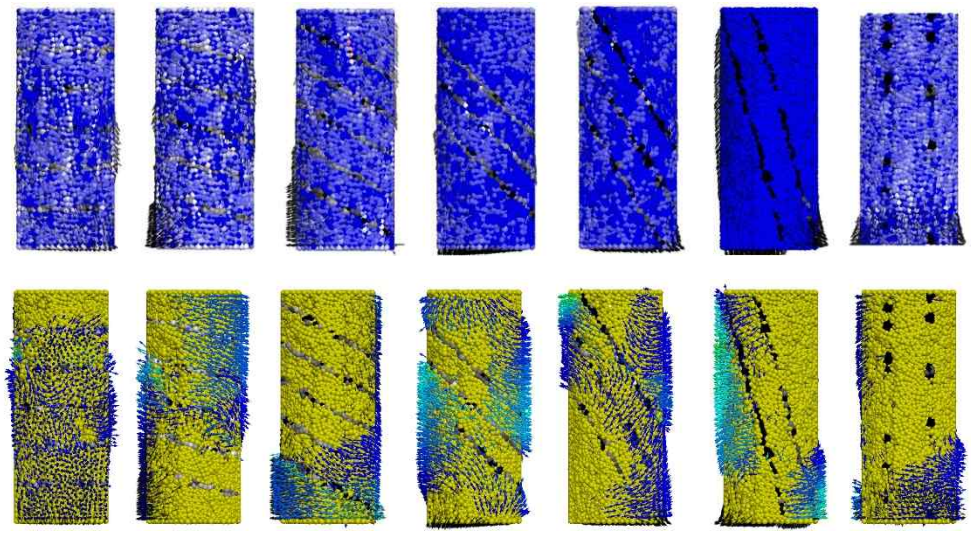

(b)

Fig. 5.2 Transversely isotropic PFC model (a) UCS test result (b) and outcome

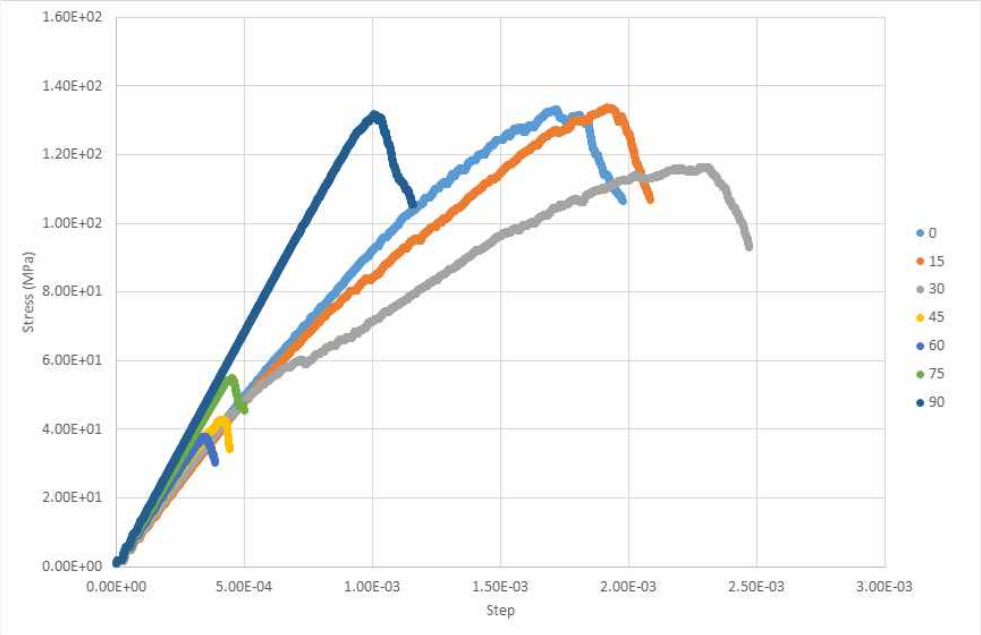

Fig. 5.3 Stress-strain curve of transversely isotropic PFC model

The maximum and minimum values of the strength derived from the analysis were also measured to be minimum at 60° and the maximum at 0°, like the results from the laboratory experiment. However, despite the loading rate has been controlled as much as 10^2 times in difference as in 0.15 mm/s and 0.0015 mm/s, strength of the model specimen failed to show such difference. As test results shown in Table 5.2, strength of two tests were simulated to have less than 1% of difference in average. The biggest strength difference could be found at 75° in which the strength of faster loading was 53.42 MPa which was 5.78% lower than that of 56.51 MPa in slower loading.

Through these results, it could be known that the change of loading or strain rate within the same micro parameters did not conclude in change of strength. Moreover, it could be noted that PFC3D was not an appropriate software tool to research dependency of strength for models with same micro

parameters.

Table 5.2 PFC3D UCS Results

Angle		0	15	30	45	60	75	90
UCS (MPa)	0.15 mm/s	133.15	133.69	116.33	42.88	37.73	56.51	131.74
	0.0015 mm/s	135.57	133.53	115.81	42.65	37.19	53.42	132.10

Chapter 6. Conclusions

This study focuses on the strength characteristics of transversely isotropic rocks under static load conditions and compressive load at intermediate strain rates. Expression of transverse isotropic characteristics according to loading rates were investigated using Boryeong schist, cement mortar, and 3D printed specimens. In addition, the smooth-joint contact model was applied using PFC3D, a commercial program using the DEM-based particle bonding model, to simulate the transversely isotropic properties and reproduce the laboratory test results. The results of the load test using a hydraulic pressure loading machine, drop weight test machine and the DEM numerical simulation on the manufactured specimens with degree of anisotropy of 0, 15, 30, 45, 60, 75, and 90 degrees are as followed.

(1) As a result of testing by manufacturing samples with two different mixing ratios of cement to form alternating layers, the maximum strength was measured as the angle between the loading direction and the isotropic plane of the specimen was closer to 0 and 90 degrees. The minimum strength was measured as the degree of anisotropy was near 45 and 60 degrees, the 'U' shape of strength according to the degree of anisotropy was confirmed, also confirming that the cement mortar specimen artificially manufactured alternating layer had transversely isotropic behavior. The test using a loading machine and a drop weight machine tried to confirm the change in strength and anisotropic characteristics according to the range of loading rate, but only the quantitative relationship according to the difference in loading rate under the same testing method could be confirmed.

(2) Since the 3D printed specimen was printed with a single material, it was impossible to prepare a sample that forms an alternating layer like the cement mortar test specimen. On the other hand, the discontinuity was expressed by modeling 1 mm × 1 mm × 1 mm grid pattern. Since it is known that acrylic resin material exhibits brittle fracturing behavior in very low temperature environment, all tests were conducted in dry ice condition. It was also possible to confirm the ‘U’ shape of strength according to the degree of anisotropy of the 3D printed specimen. Changes in strength and anisotropic behavior according to the difference in loading rate were also confirmed by the tests using a loading machine and a drop weight machine. However, in the drop weight test, specimens with weaker strength compared to the specimens used with loading machine tests was used. Only quantitative relationships could be confirmed via tests.

(3) In case of Boryeong schist, discontinuity appears alternately, and it has been confirmed through several previous studies that it has transversely isotropic properties. The Boryeong schist used in this study was also able to confirm the 'U' shape of the strength according to the degree of anisotropy, but it was not possible to derive a quantified result along 15 degrees as other artificial samples according to the nature of rock. Only a quantitative relationship according to the change in the loading rate under the same testing method could be confirmed.

(4) With the PFC3D program, a DEM based particle bonding model, this study tried to reproduce the laboratory test result for each loading rate. However, only the results reproduced under static loading conditions could be confirmed to match the actual test results. The analysis was performed using the loading rates of 0.15 mm/s and 0.0015 mm/s, which are in range of

quasi-static strain rate loading, but no change of strength in simulation was confirmed. The intermediate strain rate testing was reproduced at a loading rate of 150 mm/s in the model of same physical properties, but the test simulation failed. On the other hand, in the simulated test results reproduced at quasi-static strain rates, the ‘U’ shape of strengths according to the degree of anisotropy could be confirmed just like the results of the laboratory tests. In order to derive a quantitative relationship with the laboratory test results through numerical simulation, sufficient micro property correction should be made to reproduce the results of the compression tests under intermediate strain rate.

Through this study, examining the behavior of transversely isotropic properties and the changes in strength of the specimens according to the different loading rate, it was confirmed that the expression of anisotropic property decreased with the increase of the strain rate. On the other hand, in the case of drop weight test with the faster strain rate loading, it failed to confirm quantitative increase in strength compared to the test results from a loading machine. It could not be confirmed through tests that change in strength occurs according to change in strain rate loading in this study. However, in the future, sufficient additional tests should be conducted so that static and dynamic loading tests using various testing methods can derive quantitative strength test results according to the loading speed.

References

Brady, B.H., Brown, E.T., 1993. Rock Mechanics: for Underground Mining. Springer.

Cundall, P.A., 2001. A discontinuous future for numerical modelling in geomechanics? Proceedings of the Institution of Civil Engineers - Geotechnical Engineering 149, 41-47.

Donath, F.A., 1972. Effects of cohesion and granularity on deformational behavior of anisotropic rock. Studies in Mineralogy and Precambrian Geology 135, 95-128.

Gholami, R., Rasouli, V., 2013. Mechanical and elastic properties of transversely isotropic slate. Rock Mechanics and Rock Engineering 47, 1763-1773.

Goodman, R.E., 1989. Introduction to Rock Mechanics. Wiley New York.

Hogan, J.D., Boonsue, S., Spray, J.G., Rogers, R.J., 2012. Micro-scale deformation of gypsum during micro-indentation loading. International Journal of Rock Mechanics and Mining Sciences 54, 140-149.

Itasca, C., 2008. User's guide in PFC3D version 4.0 [M]. Minneapolis: Itasca Consulting Group Inc.

Jaeger, J.C., 1960. Shear Failure of anistropic rocks. Geological Magazine 97, 65-72.

Jung, H.-R., Kim, J.-W., 2006. Deformation behaviors around tunnel in anisotropic rocks considering joint orientation and rock pressure condition using scaled model tests. Journal of Korean Society for Rock Mechanics 16, 313-325.

Mas Ivars, D., Pierce, M.E., Darcel, C., Reyes-Montes, J., Potyondy, D.O., Paul Young, R., Cundall, P.A., 2011. The synthetic rock mass approach for jointed rock mass modelling. International Journal of Rock Mechanics and Mining Sciences 48, 219-244.

Mas Ivars, D., Potyondy, D., Pierce, M., Cundall, P.A., 2008. The Smooth-Joint Contact Model. 8th WCCM and 5th ECCMASE. Venice, Italy.

Muralha, J., Grasselli, G., Tatone, B., Blümel, M., Chryssanthakis, P., Yujing, J., 2013. ISRM Suggested Method for Laboratory Determination of the Shear Strength of Rock Joints: Revised Version. Rock Mechanics and Rock Engineering 47, 291-302.

Park, B., Min, K.-B., 2012. Discrete element modelling of shale as a transversely isotropic rock, Proceedings of ISRM Regional Symposium-7th Asian Rock Mechanics Symposium. OnePetro. 336-342

Park, B., Min, K.-B., Thompson, N., Horsrud, P., 2018. Three-dimensional bonded-particle discrete element modeling of mechanical behavior of transversely isotropic rock. International Journal of Rock Mechanics and Mining Sciences 110, 120-132.

Potyondy, D.O., 2010. A grain-based model for rock: approaching the true microstructure. Proceedings of Rock Mechanics in the Nordic Countries, 9-12.

Potyondy, D.O., 2015. The bonded-particle model as a tool for rock mechanics research and application: current trends and future directions. Geosystem Engineering 18, 1-28.

Potyondy, D.O., Cundall, P.A., 2004. A bonded-particle model for rock. International Journal of Rock Mechanics and Mining Sciences 41, 1329-1364.

Reddish, D., Stace, L., Vanichkobchinda, P., Whittles, D., 2005. Numerical simulation of the dynamic impact breakage testing of rock. International Journal of Rock Mechanics and Mining Sciences 42, 167-176.

Shen, P., Tang, H., Zhang, B., Ning, Y., He, C., 2021. Investigation on the fracture and mechanical behaviors of simulated transversely isotropic rock made of two interbedded materials. Engineering Geology 286.

Tien, Y.M., Kuo, M.C., Juang, C.H., 2006. An experimental investigation of the failure mechanism of simulated transversely isotropic rocks. International Journal of Rock Mechanics and Mining Sciences 43, 1163-1181.

Whittles, D., Kingman, S., Lowndes, I., Jackson, K., 2006. Laboratory and numerical investigation into the characteristics of rock fragmentation. Minerals Engineering 19, 1418-1429.

Wicaksana, Y., Jeon, S., 2020. Mechanical behaviour of rock subjected to uniaxial compression at intermediate strain rate. Geosystem Engineering 23, 243-250.

Yao, N., Ye, Y.-C., Hu, B., Wang, W.-Q., Wang, Q.-H., 2019. Particle Flow Code modeling of the mechanical behavior of layered rock under uniaxial compression. Archives of Mining Sciences 64, 181-193.

Zhang, Q.B., Zhao, J., 2014. A review of dynamic experimental techniques and mechanical behaviour of rock materials. Rock Mechanics and Rock Engineering 47, 1411-1478.

Zhou, T., Zhu, J., 2018. Identification of a suitable 3D printing material for mimicking brittle and hard rocks and its brittleness enhancements. Rock Mechanics and Rock Engineering 51, 765-777.

초 록

암석은 높은 강도와 취성 파괴거동을 보이는 특성을 갖는다. 암석의 굴착은 대부분 발파와 기계식 굴착으로 진행되며 이 경우 암석은 높은 변형률속도에 노출된다. 특히, 암석의 기계식 굴착 장비를 활용한 암석의 굴착에서 암석이 절삭공구의 이동 혹은 회전에 의하여 굴착 될 시 암석은 중간변형률속도의 하중 재하를 받는 것으로 보고된 바 있다. 암반의 기계식 굴착에서 절삭효율은 불연속면의 상태에 의하여 영향을 받으며 특히 불연속면의 밀도 및 굴착 방향과 불연속면이 이루는 방향에 큰 영향을 받는다. 반면, 재하속도의 변화에 따라 암석의 변형 및 파괴 거동이 달라지게 되며, 높은 재하속도에서는 상대적으로 높은 강도와 낮은 이방성 특성이 발현되는 것으로 알려져 있다.

이 연구에서는 횡등방성 암석과 유사 시험편을 사용하여, 정하중 조건과 중간 변형률속도의 압축하중 상태에서 시험편의 강도 특성을 고찰하고자 하였다.
횡등방성 암석의 압축강도는 하중방향과 등방축이 이루는 각도의 변화에 따라 U형의 특성이 나타남이 이론적, 실험적으로 알려져 있는 바, 하중 속도, 즉 변형률속도를 달리할 때 그 형태의 변화를 고찰하고자 하였다. 시험편으로는 보령편암, 횡등방성을 갖도록 제작된 시멘트모르타르 및 3D프린터 출력물을 이용하였다. 시멘트모르타르 시험편은 시멘트와 주문진표준사를 중량비 100:0, 70:30로 2종을 배합하여 10 mm 두께의 교호층을 이루도록 제작하였으며, 이때 시험편의 축방향과 등방축이 0, 15, 30, 45, 60, 75, 90도의 각도를 갖도록 하였다. 3D프린터 출력물은 Stratasys사 Objet 30 Pro 프린터 및 투명 PMMA재료인 Veroclear를 사용하여 제작하였으며, 1 mm 간격의 격자무늬를 연약층으로 하고 이를 10 mm 간격으로 배열한 횡등방성 시험편으로 제작하였으며 이방성 각도는

시멘트모르타르 시험편과 동일하도록 하였다. 하중 조건으로 3가지를 설정하였으며, 만능시험기 MTS하중기를 이용한 정하중과 동하중(재하속도 0.0067 mm/s, 10 mm/s)의 단축압축시험과 자유낙하시험기를 이용한 동하중 시험을 실시하였다. 하중기기 시험 결과, 0°, 90°에 가까워질수록 최대 강도가 측정되었으며 45°, 60°에 가까워질수록 최소 강도값이 측정되었다. 최대, 최소강도의 변화 양상은 유지하였으나 정하중(0.0067 mm/s재하)에서의 강도보다 동하중(10 mm/s 재하)에서의 강도가 최소강도는 약 15%, 최대강도는 약 3% 증가하여 높은 재하속도에서 최소 및 최대강도 사이의 편차가 줄어들었음을 확인하였다.

PFC3D(Particle Flow Code 3D)를 이용한 수치모사를 통하여 실내 시험결과와 재현된 결과를 비교하여 정량적인 관계를 도출하고자 하였다. 해석은 유압식 가압장치를 사용하는 Quasi-static수준의 변형률속도인 0.15 mm/s 와 0.0015 mm/s의 재하속도로 가압하였다. 실내실험의 결과와 마찬가지로 45°, 60°에 가까워질수록 강도의 최소값이 측정되었으며 0°, 90°에 가까워질수록 강도의 최대값이 관찰되었다.

주요어: 횡등방성, 중간변형률속도, 파괴강도, 보령편암, 시멘트모르타르, 3D프린터

학 번: 2019-24903